21021

NATIONAL LIBRARY
OTTAWA

BIBLIOTHÈQUE NATIONALE
OTTAWA

NAME OF AUTHOR. PAUL R. H. GUTOWSKI

TITLE OF THESIS. SEISMIC ARRAY INVESTIGATIONS OF THE UPPER AND LOWER MANTLE

UNIVERSITY. U. OF ALBERTA, EDMONTON

DEGREE FOR WHICH THESIS WAS PRESENTED. Ph.D.

YEAR THIS DEGREE GRANTED. 1974

Permission is hereby granted to THE NATIONAL LIBRARY OF CANADA to microfilm this thesis and to lend or sell copies of the film.

The author reserves other publication rights, and neither the thesis nor extensive extracts from it may be printed or otherwise reproduced without the author's written permission.

(Signed) Paul R. Gutowski

PERMANENT ADDRESS:

#42, 8735-165 St.
EDMONTON, ALTA.

DATED. JAN. 30 1974

NL-91 (10-68)

THE UNIVERSITY OF ALBERTA

# SEISMIC ARRAY INVESTIGATIONS OF THE UPPER AND LOWER MANTLE

by

© PAUL RAMSDEN HENRYK GUTOWSKI

A THESIS

SUBMITTED TO THE FACULTY OF GRADUATE STUDIES AND RESEARCH

IN PARTIAL FULFILLMENT OF THE REQUIREMENTS FOR THE DEGREE

OF DOCTOR OF PHILOSOPHY

DEPARTMENT OF PHYSICS

EDMONTON, ALBERTA

SPRING, 1974

THE UNIVERSITY OF ALBERTA

FACULTY OF GRADUATE STUDIES AND RESEARCH

The undersigned certify that they have read, and recommend to the Faculty of Graduate Studies and Research, for acceptance, a thesis entitled SEISMIC ARRAY INVESTIGATIONS OF THE UPPER AND LOWER MANTLE submitted by Paul Ramsden Henryk Gutowski in partial fulfillment of the requirements for the degree of Doctor of Philosophy.

E. R. Kanasewich
Supervisor

G. C. Gunning

W. G. Laver

M. L. Evans

R. S. Johnston

Wayne Thatcher
External Examiner

Date JANUARY 24, 1974

## ABSTRACT

The variable aperture seismic array (VASA) is used to investigate the upper and lower mantle of the earth by measuring $dT/d\Delta$ and the azimuth of arriving body wave phases.

To study upper mantle structure a form of coherency velocity spectral analysis employing a zero lag cross-correlation technique which scans seismic channels in slowness, time, and azimuth has been applied to the P codas of a number of teleseismic events collected by VASA during 1970. This method has revealed systematic patterns of arriving energy which may be attributable to reflections of the P wave off discontinuities in the upper mantle in the depth range of 130 km to 170 km, and at 660 km. Additionally, these patterns seem to contain information concerning the source of the earthquake.

VASA and the other University of Alberta array, Peace, and the three Canadian network seismic stations, EDM, FSJ, and MCC have been used to make $dT/d\Delta$ determinations at distances of 80° - 95°. Earthquakes from Japan, Asia, and South America have small travel time station anomalies and phase velocities that are in good agreement with the Jeffreys-Bullen tables. Events from Tonga and Samoa have phase velocities that are up to 15% higher. The inclusion of the azimuthal deviations of

South Pacific events at VASA and LASA permits the anomaly to be interpreted as a heterogeneous region of high velocity in the mantle at the core-mantle interface with a surface projection lying northeast of the island of Hawaii.

ACKNOWLEDGEMENTS

I would like to take this opportunity of expressing my thanks and appreciation to the following persons who were instrumental in the completion of this work:

To my supervisor, Dr. E.R. Kanasewich, who originally interested me in seismology, who unhesitatingly provided guidance and assistance throughout every phase of this work, and who, I suspect, will continue to live with the consequences of my years at the University of Alberta. Many thanks, Ernie.

To Dr. C.H. Chapman, for a number of discussions on the seismic inverse problem and the behavior of waves in regions of inhomogeneity which came to mind during the writing of this work and for the use of his travel time program upon which many of the theoretical curves in this study are based.

To Dr. R.M. Ellis, who provided much encouragement and assistance during the initial stages of this work, who wrote a number of programs to facilitate data preparation, and who shared in the completion of this somewhat tiresome phase.

To my friend and sometime co-worker, Tumër Alpaslan for sharing a number of his ideas and programs.

To Mrs. Mary Yiu who, after suffering my bad writing and "rush" changes, did such a beautiful job in typing the manuscript.

To the University of Alberta and the Province of Alberta whose financial support in the form of G.T.A.'s and, in the final year, a Dissertation Fellowship enabled me to obtain my education and complete this work.

TABLE OF CONTENTS


| | | Page |
|---|---|---|
| CHAPTER I : | THE SEISMIC ARRAY | 1 |
| 1. | The Use of the Array | 1 |
| 2. | Recording Instrumentation and Array Data Preparation | 4 |
| CHAPTER II : | VELOCITY SPECTRAL STUDIES OF UPPER MANTLE STRUCTURE | 14 |
| 1. | Introduction | 14 |
| 2. | Coherency Velocity Spectral Analysis | 14 |
| 3. | Observations | 24 |
| 4. | Interpretation | 40 |
| 5. | Conclusion | 47 |
| CHAPTER III : | SEISMIC ARRAY EVIDENCE FOR A LOWER MANTLE HETEROGENEITY BENEATH THE ISLAND OF HAWAII | 49 |
| 1. | Introduction | 49 |
| 2. | Array Determined $dT/d\Delta$ Methods and $dT/d\Delta$ Observational Results | 50 |
| 3. | Interpretation | 82 |
| CHAPTER IV : | THE HAWAIIAN LINEAR VOLCANIC CHAIN AND ITS POSSIBLE ORIGIN | 92 |
| 1. | Introduction | 92 |
| 2. | Surface Description of the Hawaiian Linear Volcanic Chain | 93 |
| 3. | Geochronology of the Hawaiian-Emperor Chain | 94 |

| | | | Page |
|---|---|---|---|
| CHAPTER IV | : | (cont'd) | |
| | 4. | Subsurface Data of Hawaii | 96 |
| | 5. | Origins of the Hawaiian Linear Volcanic Chain | 101 |
| | 6. | Worldwide Nature of Hot Spots and Controversies | 103 |
| | 7. | Conclusion | 108 |
| BIBLIOGRAPHY | | | 110 |
| APPENDIX | : | The Covespa Program | 120 |

## LIST OF TABLES


| | | Page |
|---|---|---|
| Table 1. | The Time Differences Between pdpP and P Phases for Various Values of d. | 46 |
| Table 2. | Differences between Observed Travel Times at VASA and the J-B Tables | 70 |
| Table 3. | Ages of the Hawaiian Islands as a Function of Distance from Kilauea | 95 |

LIST OF FIGURES


| | | Page |
|---|---|---|
| Figure 1. | The Location of the Seismic Arrays | 7 |
| Figure 2. | Block Diagram of the Tripartite System | 9 |
| Figure 3. | Response of the Recording System | 11 |
| Figure 4. | Amplitude Induced Variation in Sidelobe Pattern | 19 |
| Figure 5. | Effect of High Coherency Values | 21 |
| Figure 6. | Effect of Prolonged Wavetrain on a Covespagram | 23 |
| Figure 7. | Azimuthal Response of Covespa with VASA | 26 |
| Figure 8. | Covespagram of Event 64 (Tonga) | 29 |
| Figure 9. | Extended Covespagram | 32 |
| Figure 10. | Covespagram of Event 88 (Tonga) | 35 |
| Figure 11. | Covespagram of Event 72 (New Ireland) | 37 |
| Figure 12. | Covespagram of Event 74 (Hindu Kush) | 39 |
| Figure 13. | Ray Diagram Showing Phase pdpP | 45 |
| Figure 14. | Three Station Velocity-Azimuth Determination | 53 |
| Figure 15. | Event 88 Record Suite | 61 |
| Figure 16. | Worldwide $dT/d\Delta$ Results for VASA | 63 |
| Figure 17. | Expanded $dT/d\Delta$ Results for VASA, FSJ-Peace, and MCC-EDM Arrays with Velocity Model | 66 |
| Figure 18. | LASA P-Wave Phase Velocities | 68 |
| Figure 19. | View of South Pacific Showing the Earthquake Sources, Receivers, and Ray Turning Points | 73 |

Page

Figure 20. Expanded View of Projected Turning Points 76

Figure 21. S-Wave Phase Velocities 79

Figure 22. Comparison of 'Normal' and 'Anomalous' Waveforms. 88

Figure 23. Sketch of Anomaly at Base of Mantle 91

Figure 24. Worldwide Plume Locations 105

# CHAPTER I

## THE SEISMIC ARRAY

### 1. The Use of the Array

In recent years the advent of the seismic array has provided geophysicists with a powerful tool for the investigation of the structure of the earth's interior. With the single station one is presented with a single record in time at any point along which there may be not one but several phases arriving simultaneously which cannot be separated and identified in time. With the array, however, one has a number of time records distributed in space so that events which arrive together in time may be separated by velocity and azimuth. This is because the small dimension of the array (of the order of 150 km) in comparison with the source-to-receiver path length results in the wave trains appearing at the individual sensors of the array being very nearly coherent. The data redundancy then lends itself to various array data processing schemes one of which will be discussed in the second chapter. In addition the array as a whole observes a "bundle" of rays which have traversed the interior of the earth in a narrow cone from the source thus permitting the detailed investigation of localized heterogeneities along this path, as will be seen

in the third chapter.

An extremely useful parameter of seismic observations is the apparent slowness $dT/d\Delta = p$, where $dT/d\Delta$ is the travel time differential with respect to distance, $\Delta$, and p is the wave parameter. The large aperture seismic array can directly measure this parameter by determining the apparent velocity (dx/dT) which is the speed and direction of the wavefronts of the body wave phases generated by an earthquake as they cross the array. The usefulness of the parameter p arises from the fact that the Wiechert-Herglotz integral (Bullen, 1963) which requires p as a function of $\Delta$ is a direct method of inverting seismic velocity-distance observations into velocity-depth profiles, providing the earth is spherically symmetric. Knowledge of the azimuth of the incoming wavefront is useful for determining the amount of deviation the ray suffers along its path and whether this deviation is large enough to rule out the assumption of the earth's approximate spherical homogeneity upon which the Wiechert-Herglotz method depends. An array having three or more sensors (of a single polarization) can measure both the apparent velocity and the azimuth of a phase independent of one another.

In order to study localized effects within the earth it is necessary to employ body waves since their

shorter wavelengths will permit greater resolution than the use of surface waves or normal modes or the long period diffracted P (Alexander and Phinney, 1966) or ScS (Mitchell and Helmberger, 1973) phases. The uniqueness of the structure as determined by inversion techniques will then depend on assumptions about the nature of low velocity channels, the completeness of the seismic data, and the proper identification of the incoming phases from sensor to sensor in the array. At teleseismic distances ($\Delta > 30°$) the apparent slowness, $dT/d\Delta$, as determined by an array is independent of the origin time of the earthquake and is only slightly dependent on source effects such as radiation patterns, near source structure, and source depth and location since one is dealing with a very narrow cone of nearly parallel rays. For an array comparable to the ones used in this study having an aperture of 150 km this solid cone of rays has angular dimensions ($d\theta.d\phi$) of 5' by 57' at a distance of 90°.

The effect of structure beneath the receiver is a more serious problem (Iyer and Healy, 1972) and can be empirically evaluated by examining events from many different azimuths and distances. This should have the effect of revealing only gross subreceiver structure since the large aperture of the array when convolved

with crustal and upper mantle variations will average out all but such gross structure (e.g. a dipping Moho).

Hence, the smaller the array aperture the more negligible will be the source $dT/d\Delta$ and azimuth effects and the more restricted will be the cone of rays into the receiver system making the resolution of structure in this cone more detailed. However, the effect of crustal structure beneath the receiver will become much greater in the case of the small array and may obscure structure encountered elsewhere along the path unless the effects are carefully studied and accounted for in the $dT/d\Delta$ results. Large aperture arrays of dimension 150-200 km seem to offer good resolution for the investigation of both upper mantle and lower mantle structure.

The methods used in this work have been used previously by Niazi and Anderson (1965), Johnson (1967, 1969), Chinnery and Toksöz (1967), Husebye et al.(1971), Husebye (1969), and Montalbetti (1971). Hales and Herrin (1972) have done a review of travel times and $dT/d\Delta$ observations.

## 2. Recording Instrumentation and Array Data Preparation

The principal network for the acquisition of teleseismic data in 1970 was the portable variable aperture seismic array (VASA). The advantage of this portable

array over the fixed array is that VASA can be repositioned to advantageous locations with respect to the earthquake epicenters. The 1970 array consisted of five stations located in central Alberta (figure 1) arranged in two equilateral triangles 160 and 30 km to the side. Each station consisted of three Willmore Mark II seismometers, a WWVB receiver, amplifiers, a multiplexer, and an analog-to-digital converter system. Figure 2 taken from Kanasewich et al. (1974) shows a block diagram of the modified tripartite digital recording gain ranging system used in 1973. However, it does contain the essential elements used in 1970. Figure 3 shows the response of the amplifier and a Willmore Mark II seismometer. This indicates that teleseismic P waves (in the frequency range 0.7 to 1.8 Hz) and S waves (about 0.2 Hz) are relatively unmodified by the system. The signal from each sensor was sampled at a rate of 12.5 times/sec and was written onto a magnetic field tape holding about two days of data. The field tapes were edited and the events passed to a station master tape.

A special WWVB timer was designed which operated by first producing 96 sec of synthetic WWVB time signal in binary pulse code format generated internally from the input hour and minute corresponding to the first minute encountered in the data block to be timed

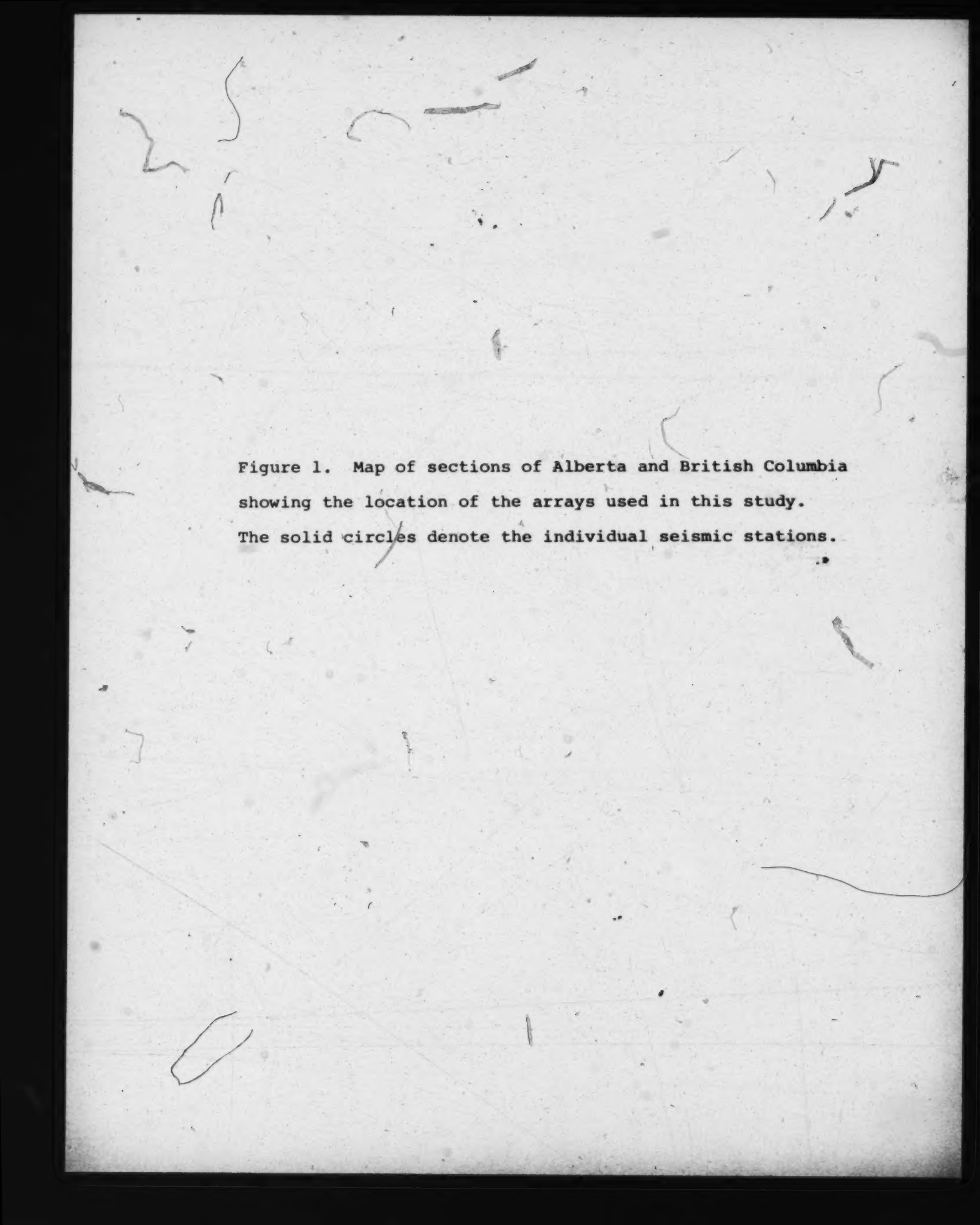

Figure 1. Map of sections of Alberta and British Columbia showing the location of the arrays used in this study. The solid circles denote the individual seismic stations.

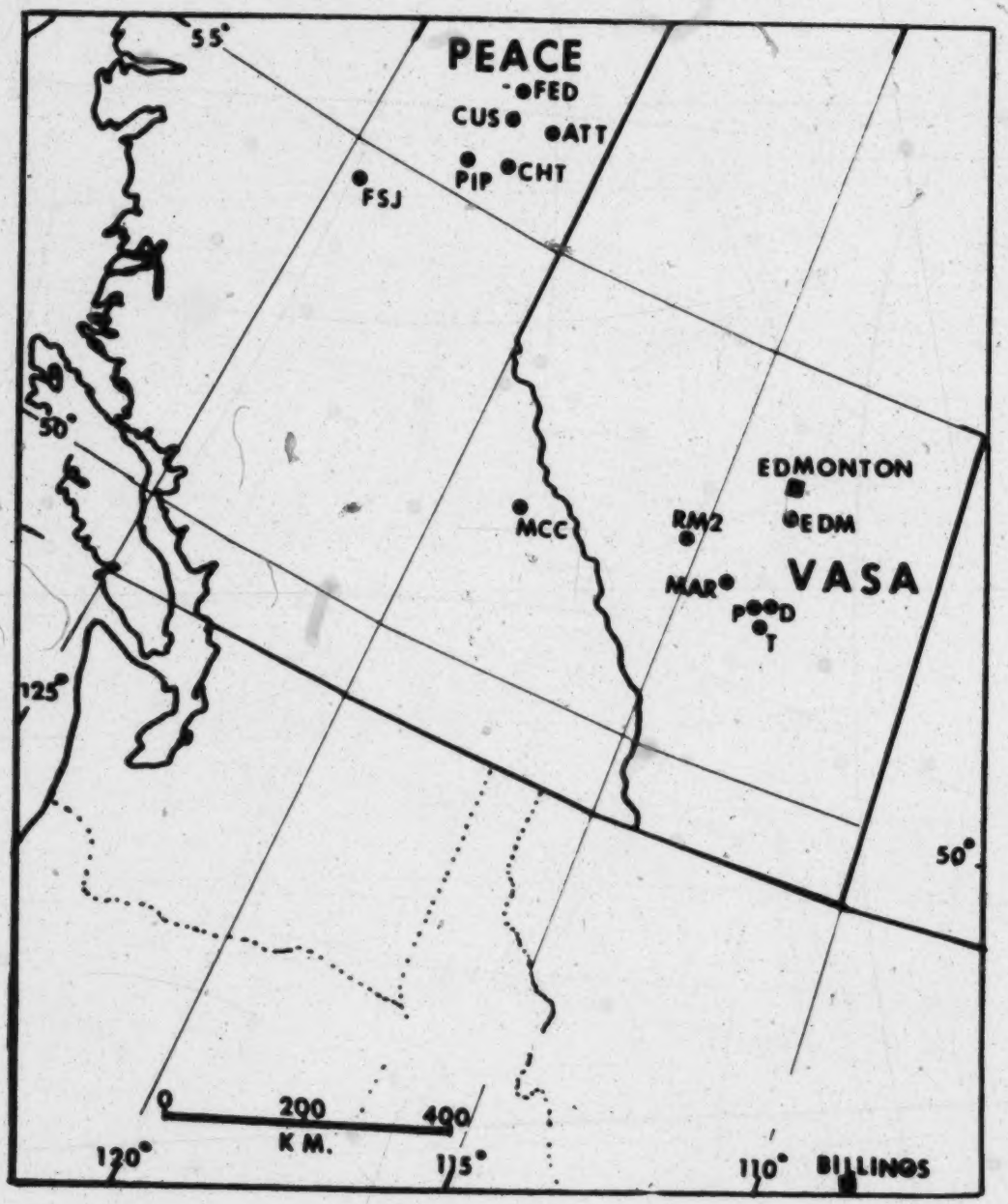
PEACE
FED
CUS
ATT
PIP
CHT
FSJ
55°
50°
125°
MCC
EDMONTON
RM2
EDM
VASA
MAR
P
D
T
50°
0
200
400
KM.
120°
115°
110°
BILLINGS

Figure 1.

Figure 2. Block diagram of the wide-band tripartite amplifier system.

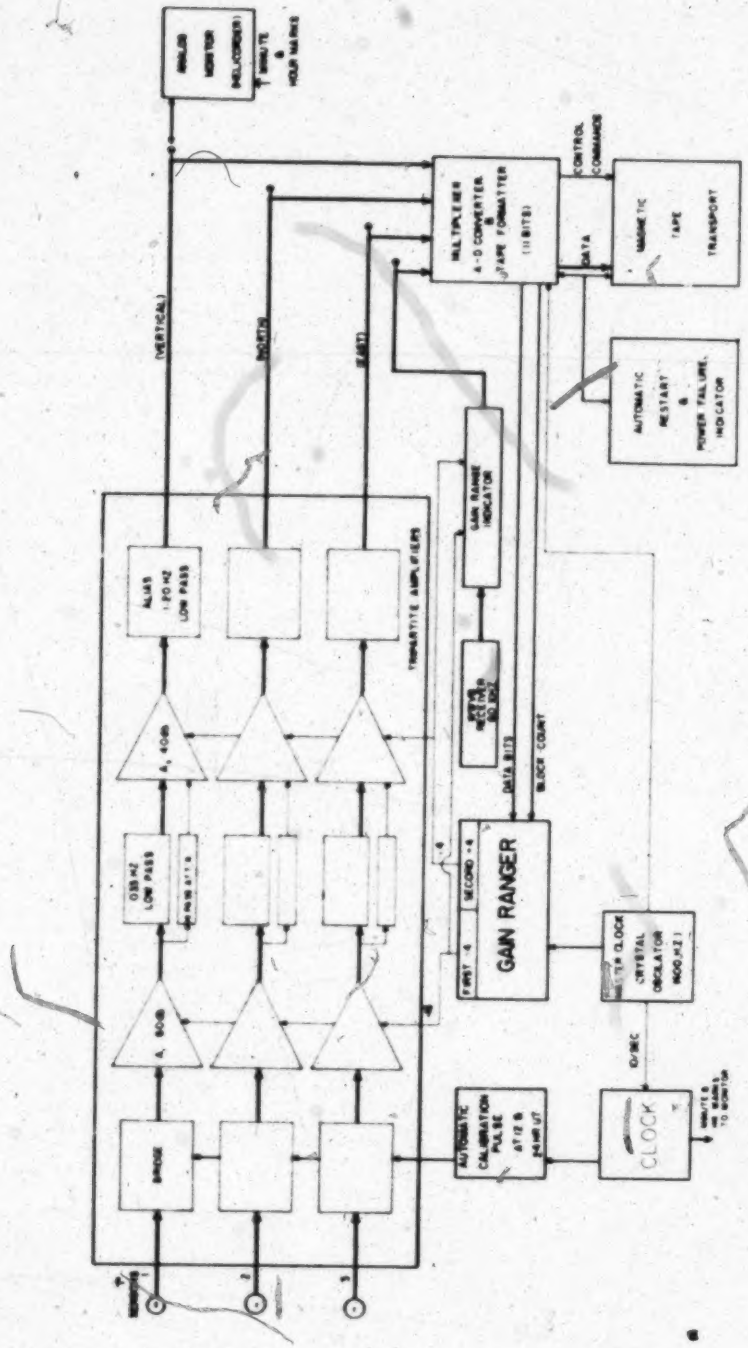
MULTIPLEXER
A-D CONVERTER
& TAPE FORMATTER
MAGNETIC TAPE TRANSPORT
CONTROL COMMANDS
DATA
AUTOMATIC RESTART & POWER FAILURE INDICATOR
(VERTICAL)
(NORTH)
(EAST)
GAIN RANGE INDICATOR
GAIN RANGER
DATA BITS
BLOCK COUNT
FIRST 4
SECOND 4
ALIAS 10 PO HZ LOW PASS
0.03 HZ LOW PASS
4, 60dB
A, 80dB
BASE
AUTOMATIC CALIBRATION PULSE
MASTER CLOCK CRYSTAL OSCILLATOR
CLOCK
0.1 SEC

Figure 2.

Figure 3. Amplifier gain of the tripartite system and the combined response of the amplifier and a Willmore Mark II seismometer.

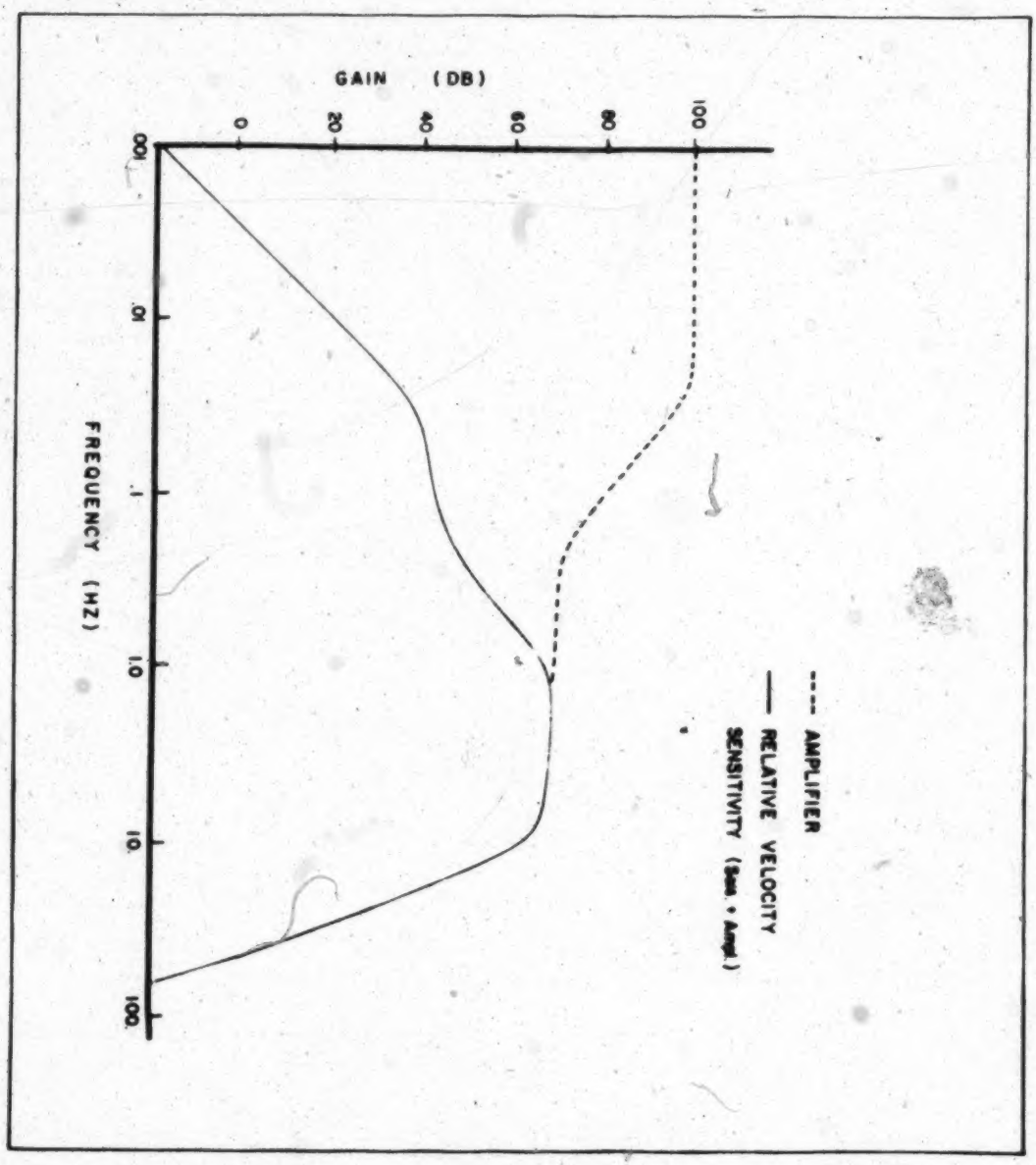
GAIN (DB)
0
20
40
60
80
100
.001
.01
.1
1.0
10
100
FREQUENCY (HZ)
---- AMPLIFIER
—— RELATIVE VELOCITY
SENSITIVITY (Sens. • Amp.)

Figure 3.

and then by cross-correlating the synthetic time signal with the actual VB signal. The maximum cross-correlation corresponded to the coincidence of the two proper minute marks and the fraction of the sampling interval or lag for which this maximum occurred was determined by a three point parabolic fit to the correlation values. Thus, from the number of lags the block start time could be determined (for good signal to noise characteristics the precision of the time determination was to within 1/4 of a sampling interval, or, in this case, 20 ms). Clearly, the accuracy of the phase times may become critical if the array is small.

Once accurate data block start times were available the events were edited such that the data for each station had exactly two minutes of noise before the Jeffreys-Bullen (J-B) predicted arrival time for that event at that station. In addition, the three traces on tape were time shifted so that they were each synchronous with the WWVB time signal. The time shift was facilitated by a simple linear interpolation procedure which incorporated a correction for the interrecord gap between blocks of data. At this stage also, the polarities of the signals were checked and any alterations made. The modified data was then written onto a final master tape with all stations reporting an event following one another and with each station having a

header card identifying the source (NOAA) and receiver (VASA) parameters. This arrangement proved to be extremely convenient for subsequent study of the events.

The second array identified in figure 2 as PEACE, is operated by the University of Alberta around the Bennett Dam on the Peace river in British Columbia and was installed in 1967 to determine the effects of crustal loading. Each station consists of one down-hole vertical seismometer the signal from which is recorded as a frequency modulation of pulses on magnetic tape. Absolute time is furnished by a WWVB receiver. The Peace array and the Canadian network station FSJ at Fort St. James, British Columbia are 220 km apart on a great circle path to the earthquake epicenters in the Tonga region. An additional two station combination was provided by the two Canadian seismic network stations EDM at Edmonton, Alberta, and MCC at Mica Creek, British Columbia.

# CHAPTER II

## VELOCITY SPECTRAL STUDIES OF UPPER MANTLE STRUCTURE

### 1. Introduction

In this chapter the concept of velocity spectral analysis which employs the coherency of the signal (Covespa) will be applied to the P codas of a number of shallow teleseismic events as detected by the variable aperture seismic array in central Alberta during 1970. The algorithm for the Covespa, using a zero lag cross-correlation technique, has been originally formulated by the geophysical exploration industry and has been modified to scan seismic array data not only in slowness (inverse velocity) and time but also in azimuth providing a "three dimensional" analysis of the data which will be called a Covespagram.

### 2. Coherency Velocity Spectral Analysis

The established ideas of velocity spectral analysis as applied to the study of seismic waves employing array data has been particularly successful in the investigation of apparent velocities (the velocities at which wavefronts appear to traverse the seismic array) and the discrimination of multiples from primary reflected energy (Schneider and Backus (1968), Taner and Koehler (1969),

Davies, Kelly, and Filson (1971)). Davies et al. have successfully employed the concept of velocity spectral analysis, Vespa, in the investigation of P waves and of core arrivals closely spaced in time. Their method has been used by Doornbos and Husebye (1972) in conjunction with the cross-correlation method of determining relative arrival times of seismic waves (this will be discussed in the next chapter) to study core phases.

The method used by Davies et al. involves the formation of a beam by delay and summation of the seismic traces of an array and the determination of the power in the beam over a specified time window which is stepped (usually in increments of 1 sec) down the resultant record. This process is then repeated for different values of slowness always keeping the beam at a constant azimuth until a two dimensional plot (Vespagram) of power in slowness and time is generated. In actual practice the array is pointed in a constant azimuth toward the source and steered over a wide range of wave slownesses so that the power in the beam of arriving waves in time may be examined.

Doornbos and Husebye (1972) have pointed out, however, that proper interpretation of the Vespagram requires knowledge not only of the response of the array as a function of slowness but also as a function

of time. The factors which determine the time response are essentially the signal variation across the array, the duration of the signal, and the asymmetry of the signal. As they have discovered, it may be difficult to properly attribute energy to a phase which follows very closely in time to a dominant arrival and is separated only in slowness due to the leakage of energy into sidelobes as a result of amplitude variations across the array.

The process incorporated in the Covespa technique involves a normalized zero lag cross-correlation which minimizes the problem of sidelobe leakage and reduces the likelihood of misinterpretation of the Covespagram by accepting only the high coherency measures. The equation is a generalization to a two dimensional array of a one dimensional form given by Montalbetti (1971),

$$CC(\phi,s,t) = \frac{2}{M(M-1).T} \sum_t \sum_k \sum_i \frac{f_{i,t}(\phi,s) \cdot f_{i+k,t}(\phi,s)}{\sqrt{\sum_t f_{i,t}^2 \cdot \sum_t f_{i+k,t}^2}} ,$$

where, CC is the coherency, M is the number of channels (or sensors) in the array, k is an incremental integer on channel i ($i \neq k$), T is the length of the time window, and $f_{i,t}$ is the amplitude of the $i^{th}$ channel at time t. The computation starts by inserting appropriate delays into the traces corresponding to a particular slowness, s, and azimuth, $\phi$. Then, for each time along the records

the zero lag cross-correlations of all combinations of two stations within a specified time window (one second for compressional, P, body waves and four seconds for transverse, S, body waves) are computed, normalized to unity and summed. Thus for an array of five stations the summation would involve 10 cross-correlation functions. Since the coherency, CC, is normalized to unity it will give a value of unity at a certain time and slowness if the phases and shapes of the signal within the window at all sensors are the same. In practice, the range of acceptable coherencies ($0.5 \leq CC \leq 1.0$) is set high enough to ensure that only similar signals, irrespective of their power, are plotted.

By using synthetic seismograms as input to the Covespa program it has been determined that although low sidelobes do exist for the variable aperture seismic array (VASA), signal strength variation causes no change in the sidelobe pattern. This is shown in figure 4 for synthetic data at a slowness of 6.0 sec/deg. The effect of using the high coherency values is shown in figure 5. 6.0 db down corresponds to a coherency of 0.5 and 20 db down corresponds to a coherency of 0.1. Figure 6 demonstrates that a prolonged wave train at all sensors merely results in an extended Covespa pattern. In addition to the slowness-time responses the effect of azimuth on the Covespagram has been determined.

Figure 4. Change in coherency pattern as a result of amplitude variation. In the first Covespagram all sensors have equal amplitudes from a synthetic event with a slowness of 6.0 sec/deg and with an azimuth of 235°. In the second Covespagram the signal amplitudes at EDM and RM2 are halved. The insert shows the approximate positioning of the array elements with respect to EDM. The coherency values are 0.9, 0.8,..., 0.5.

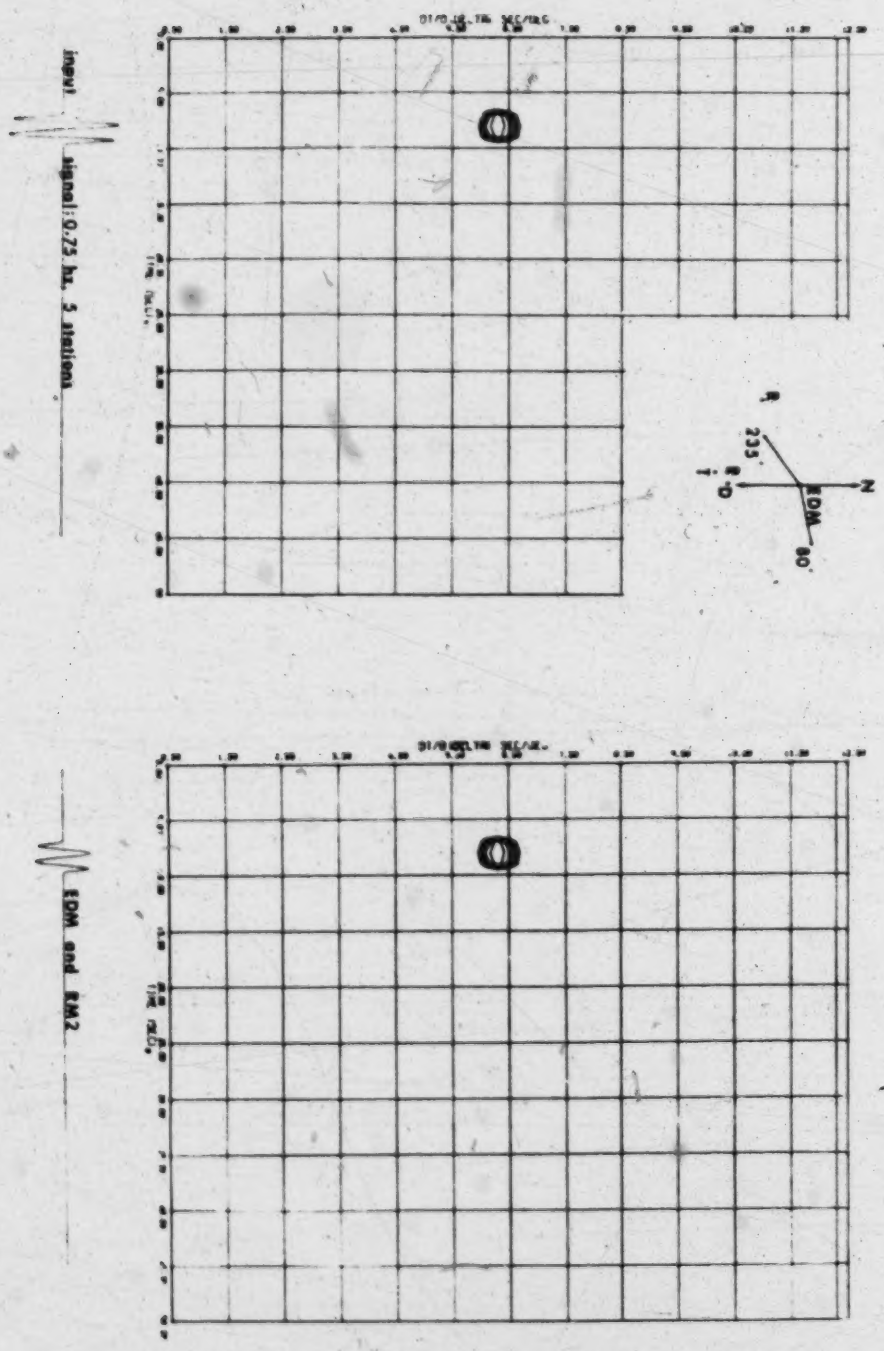
EQUAL AMPLITUDE AZIMUTH 235 DEG
EOM AND AM2 AMPLITUDE DOWN BY 0.50
input signal:0.25 hz, 5 stations
EOM and AM2
235
EOM
N
60

Figure 4.

Figure 5. The effect of choosing only high coherency values compared with the decibel scale.

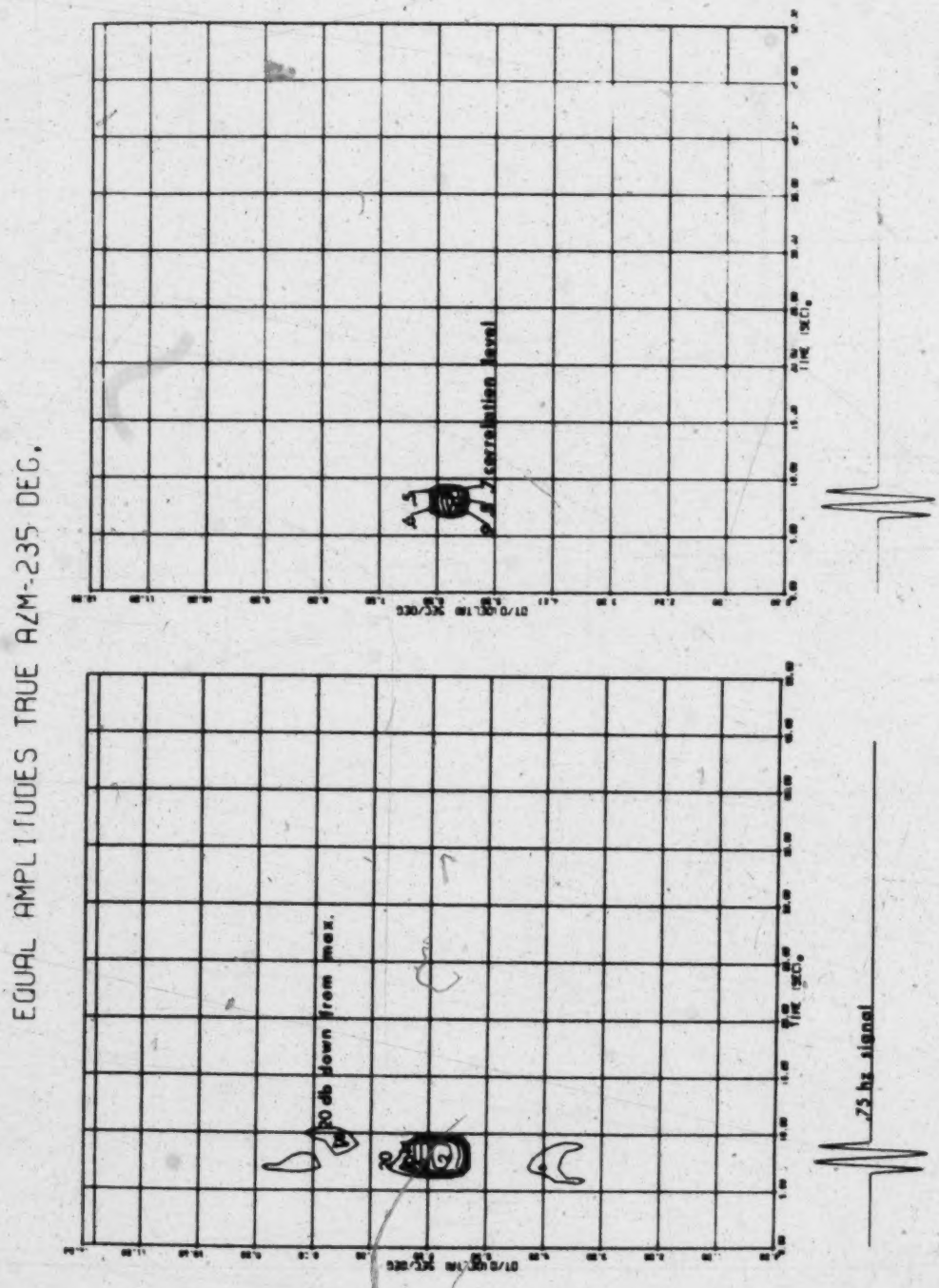
EQUAL AMPLITUDES TRUE AZM-235 DEG.
Xcorrelation level
TIME (SEC.)
-20 db down from max.
25 hz signal

Figure 5.

Figure 6. The effect of a prolonged wavetrain being directed into the array.

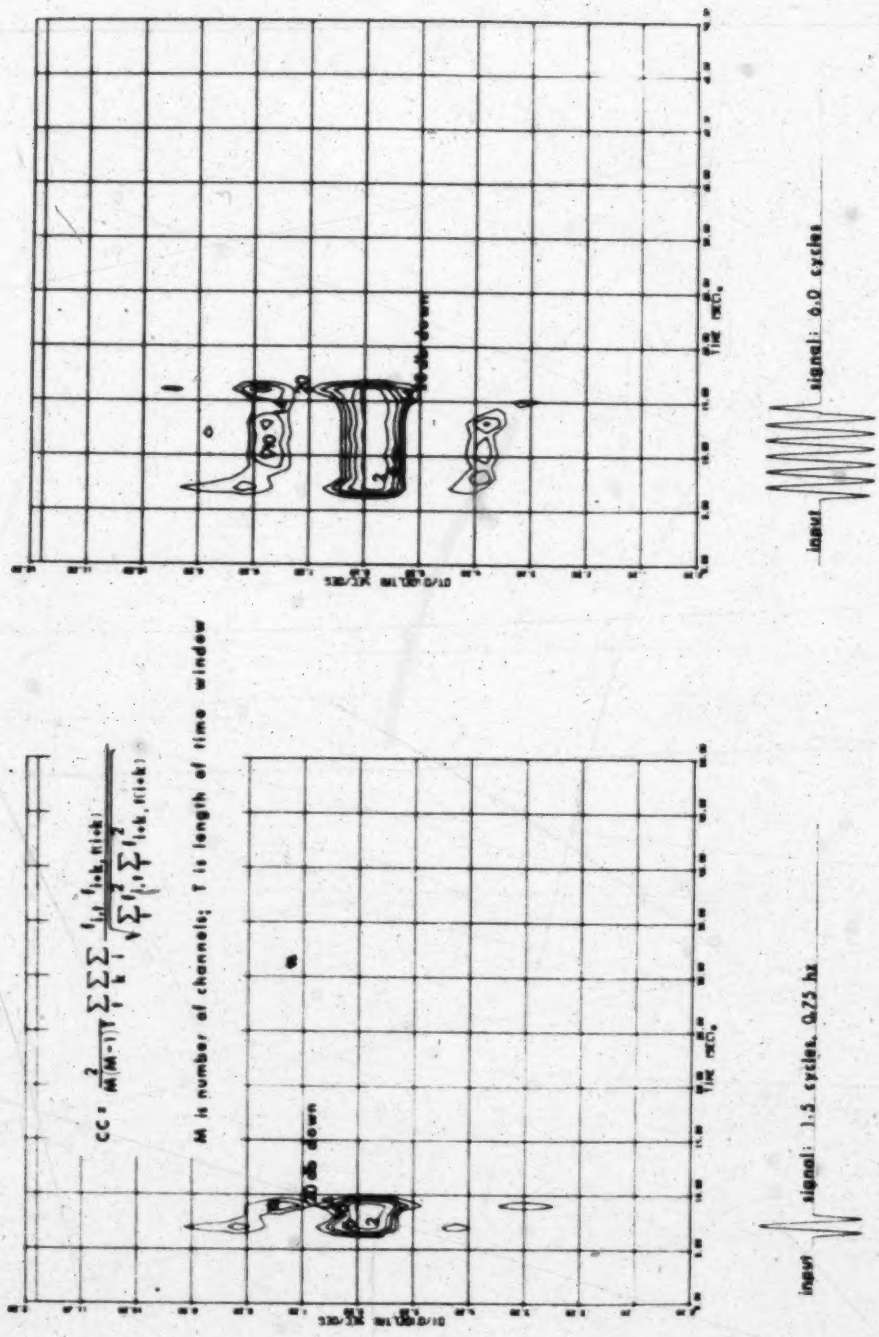
signal: 6.0 cycles
input
signal: 1.5 cycles, 0.25 hz
input
M is number of channels; T is length of time window

Figure 6.

Whitcomb (1973) has pointed out that using delay and summation (a linear process) the 10% amplitude point for LASA is ±16°. The Covespa process with the VASA array has a very sharp azimuthal response since for a synthetic event, the 10% coherence points are ±4° from the actual event direction (figure 7). Therefore, this process can be used in conjunction with VASA as an azimuth-slowness-time discriminator. This has been readily accomplished by redesigning the simple Covespa program to compute and store complete Covespagrams for a number of azimuths (in increments of say one degree) producing a "three dimensional" Covespagram (see Appendix). Then, for each coherency maximum in time the optimum slowness and azimuth are determined by parabolic curve fitting. Also, for each maximum the optimum time is determined by the same method. This procedure is then repeated for each maximum of the Covespagram in time.

## 3. Observations

The teleseismic events used in this discussion are from the South Pacific region and Asia (the azimuthal ranges being 230°- 260° and 330°- 10° respectively) and are in the epicentral distance range of 84°- 95°. These events are among the 100 events recorded by VASA during 1970 and were also used in the study of the inhomogeneity

Figure 7a. The effect of azimuth on the Covespagram as the array is steered in 1° increments on either side of the event direction (235°). The event slowness is 6.0 sec/deg. The position of the array sensors with respect to EDM is shown in the insert.

b. The array response in coherencies as a function of azimuth for the VASA 1970 array.

a

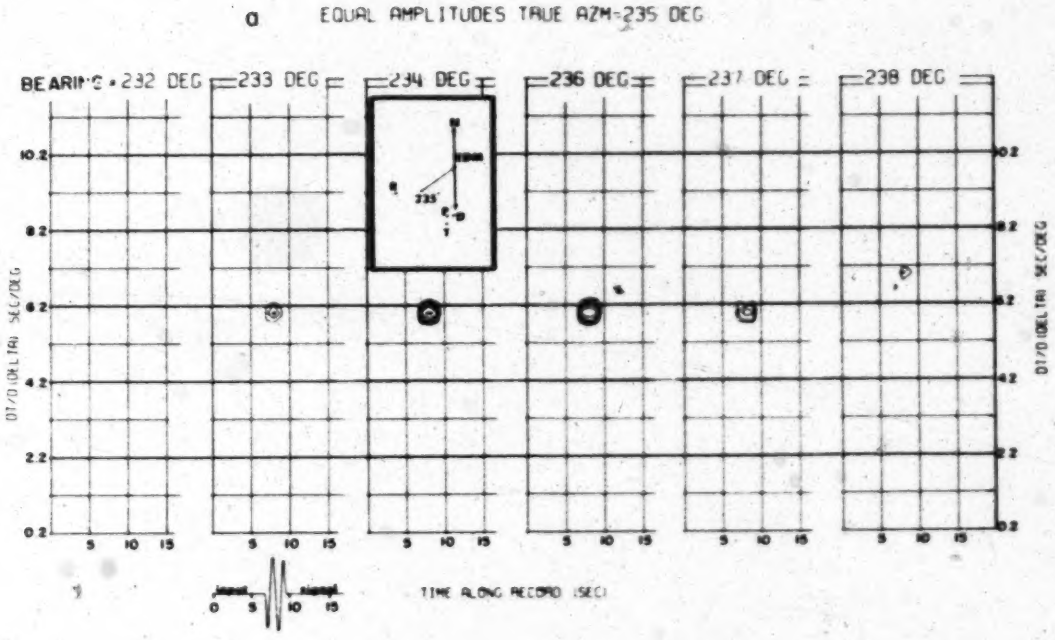
EQUAL AMPLITUDES TRUE AZM=235 DEG
BEARING = 232 DEG
233 DEG
234 DEG
236 DEG
237 DEG
238 DEG
DT/D(DELTA) SEC/DEG
TIME ALONG RECORD (SEC)

b

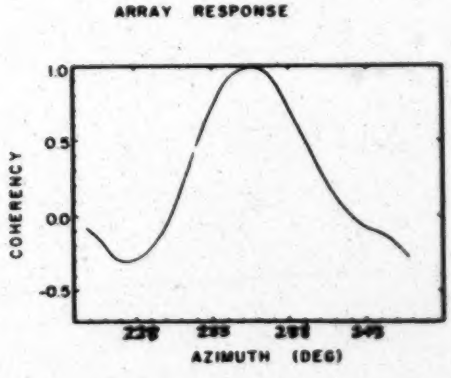
ARRAY RESPONSE
COHERENCY
1.0
0.5
0.0
-0.5
AZIMUTH (DEG)

Figure 7.

beneath the island of Hawaii at the base of the mantle (see Chapter III). All the events used in this chapter have a magnitude of 5.1 or greater.

Each of the following sets of figures contains three separate plots which have been aligned so that they relate in time. The upper plot shows the information from the azimuth-slowness-time extractor which has detected the coherency maxima of the P coda and plotted the azimuthal deviation (true bearing - geocentric azimuth) and the slowness variation on expanded scales as functions of time along the record. The solid lines joining the symbols on these plots are significant only as a visual aid. Directly beneath this plot is the Covespagram derived from the optimum azimuth depicting 100 seconds of P coda information and below this is the beam formed from the optimum azimuth and velocity. Observe that not every point in the uppermost plot coincides in time and slowness with a coherency contour on the Covespagram. The azimuthal response for this process is very sharp and because the Covespagram is generated for only one particular direction, energy arriving at an angle which deviates from that used for the Covespagram may be either suppressed or completely obliterated depending on the extent of the deviation.

Figure 8 shows event 64 which is from the Tonga region. The energy is constant in slowness and azimuth

Figure 8. Covespagram of event 64 from the Tonga Islands: $\Delta = 89°$, magnitude = 5.8, and depth = 33 km. The upper plot shows the slowness and the azimuthal deviations of the coherency maxima in time, the middle plot shows the Covespagram for one azimuth, and the third plot is the beam formed for one velocity and azimuth.

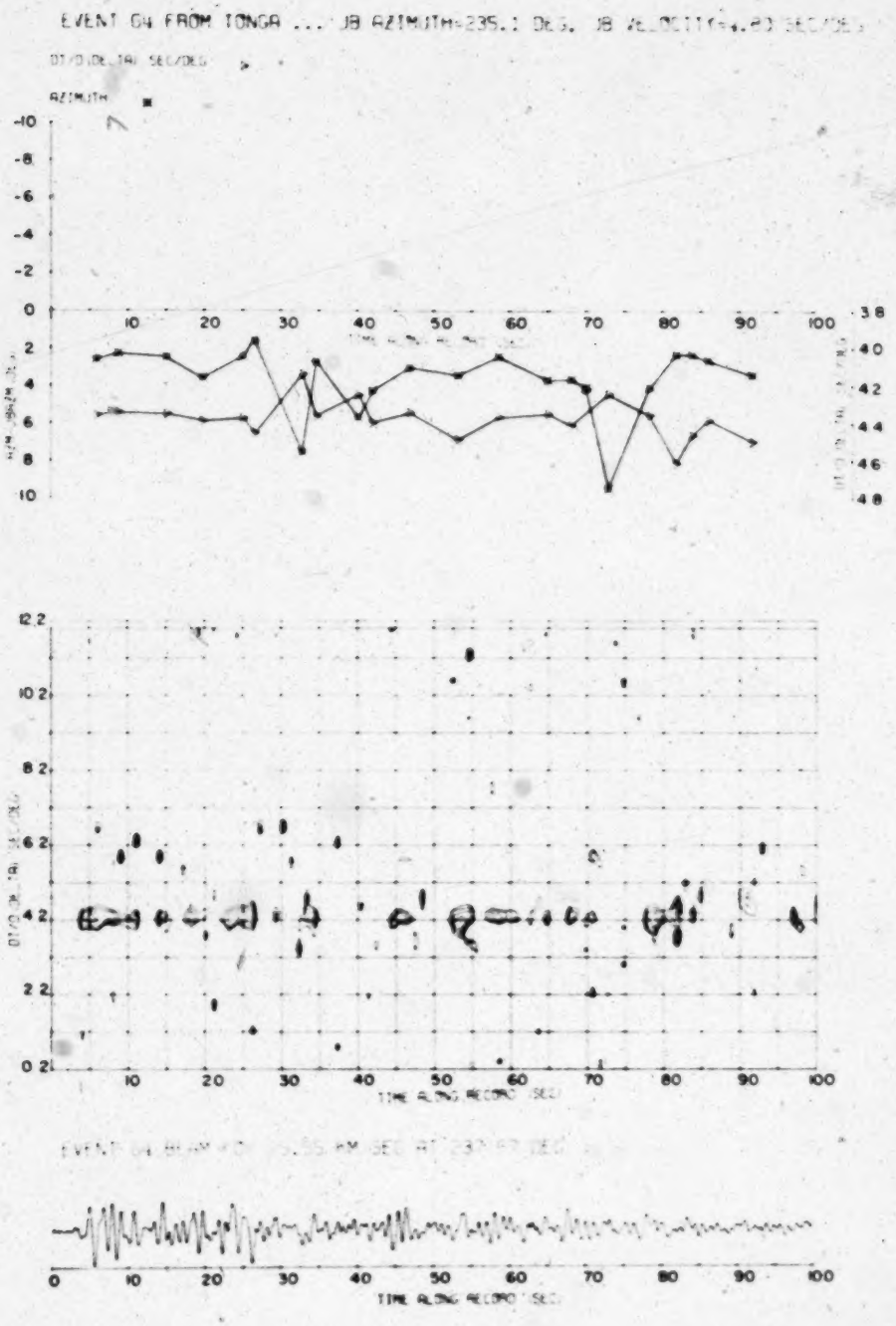
AZIMUTH
-10
-8
-6
-4
-2
0
2
4
6
8
10
10
20
30
40
50
60
70
80
90
100
38
40
42
44
46
48
12.2
10.2
8.2
6.2
4.2
2.2
0.2
TIME ALONG RECORD (SEC)

**Figure 8.**

for the first 15-20 seconds. The slowness and azimuth then exhibit systematic variations at 30 seconds and again at 70 seconds from the initial P wave arrival. The coherency contours of the Covespagram and the wave train of the beam formed trace suggest that energy arrives in groups of about 30 seconds in length repeating every 35 to 40 seconds. This trailing energy phenomenon has been seen before by Davies, Kelly, and Filson (1971).

The Covespagram of this event has been extended out to 350 seconds (figure 9) in order to better discern the individual energy groupings and the repetitive nature of their arrival. After approximately the third group the organization which seems to be inherent in this pattern begins to break down as the contours become less pronounced in time. The PP arrival should appear at about 215 seconds after the P arrival with a slowness of 8.0 sec/deg. It is possible to actually detect this phase here although it is weak, possessing a coherency level of 0.7. This weakness may in fact be due to an azimuthal shift suffered by this ray as it travelled through the upper and middle mantle regions. In addition there appear to be two strong coherencies at about 140 seconds and 148 seconds after P.

Figure 9. Extended Covespagram of event 64 with the beam showing the energy groupings. The predicted arrivals P and PP are indicated.

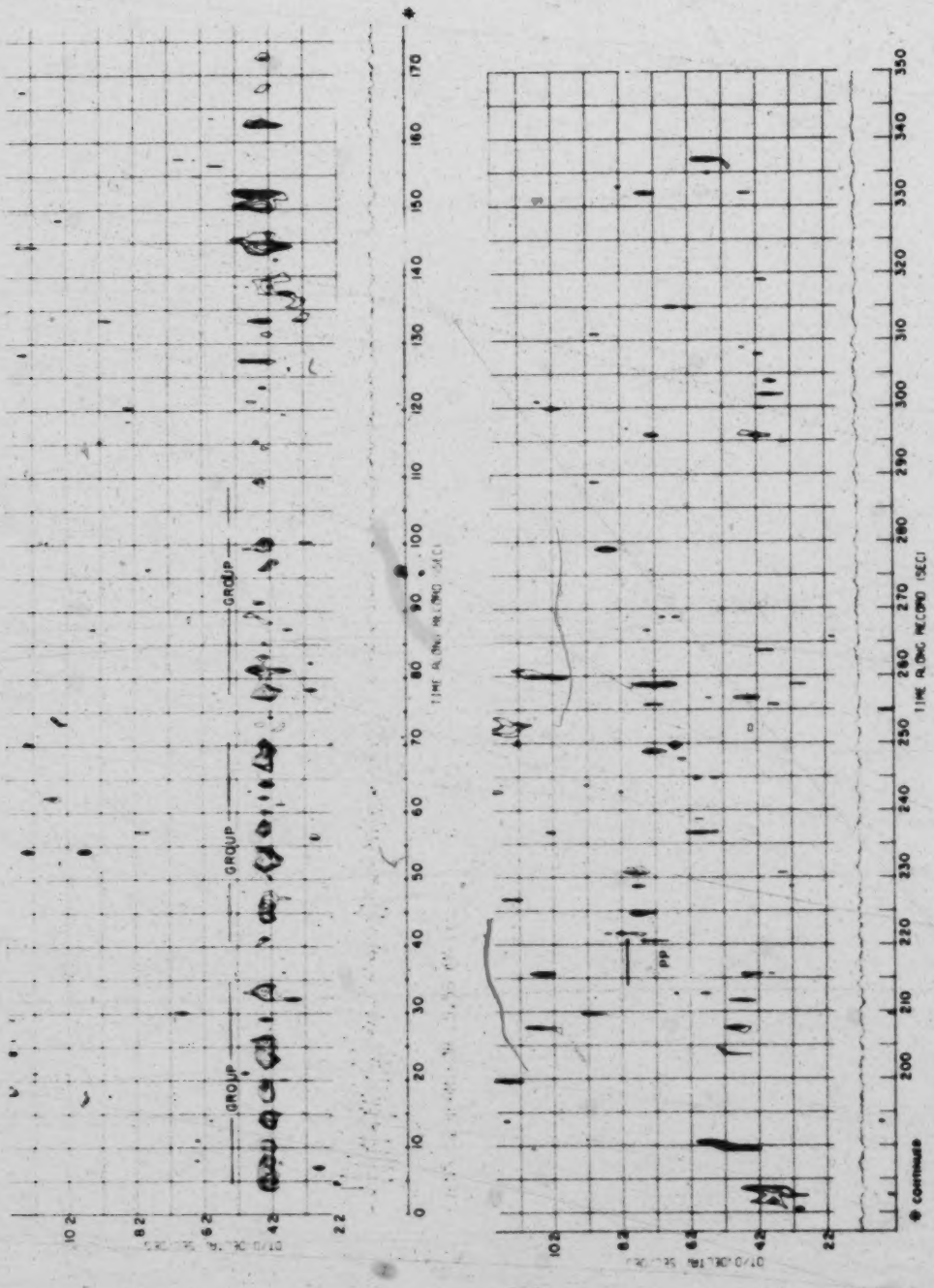
GROUP
GROUP
GROUP
PP
TIME ALONG RECORD (SEC)
TIME ALONG RECORD (SEC)
CONTINUED

Figure 9.

Event 88 (figure 10) is another Tonga event showing similar behavior to the previous case (event 64) with strong variations commencing at about 20 seconds from the initial P arrival. As is readily discerned in these figures, the slowness and azimuth deviations seem to be related. The Covespa groupings appear to be hidden further down the record as a result of strong directional variations (approximately 6° to 10°). A number of Covespagrams were computed for a sequence of azimuths and superimposed. This composite plot then revealed the familiar energy groupings repeating with a period of 40 to 45 seconds resembling very closely event 64.

Figure 11 shows an event from the New Ireland region. Here one sees very well defined coherency groupings 25 seconds or so in duration, repeating at 40 second intervals. Both the slowness and azimuth appear to be quite constant except for the azimuthal excursion at about 45 seconds.

Event 74 (figure 12) is from the Hindu Kush region (depth = 210 km) and is quite suggestive of energy groupings in spite of very strong slowness and azimuth variations. This observation taken with the broad coherency contours of the Covespagram may be indicative of extensive scattering of the wave train. This behavior seems

Figure 10. Covespagram of event 88 from the Tonga Islands: $\Delta$ = 91°, magnitude = 5.3, and depth = 33 km.

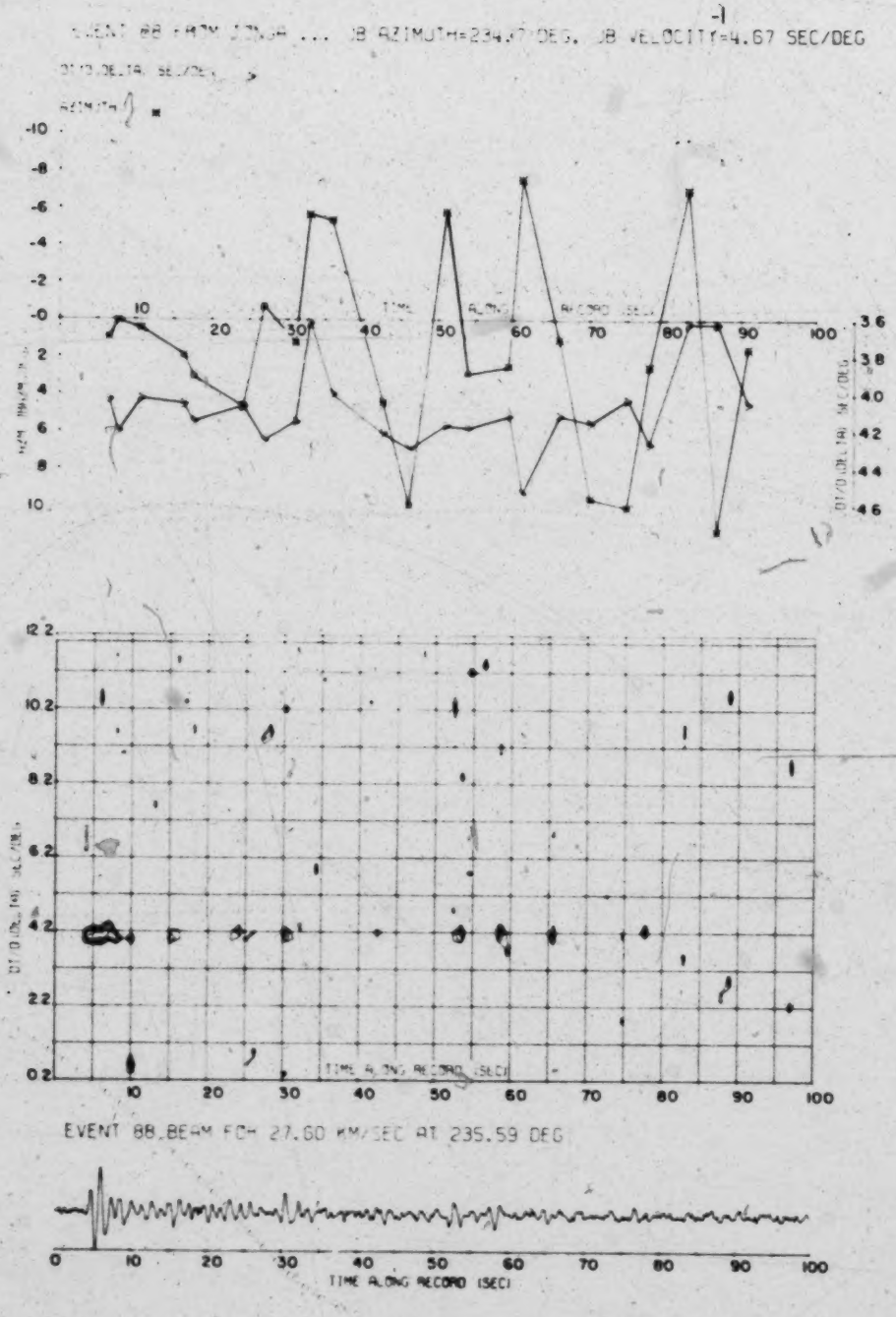
EVENT 88 FROM ICELAND ... AZIMUTH=234.7 DEG, AZ VELOCITY=4.67 SEC/DEG
AZIMUTH
TIME ALONG RECORD (SEC)
EVENT 88,BEAM FOR 27.60 KM/SEC AT 235.59 DEG
TIME ALONG RECORD (SEC)

Figure 10.

Figure 11. Covespagram of event 72 from the New Ireland region: $\Delta = 95°$, magnitude = 5.5, and depth = 20 km.

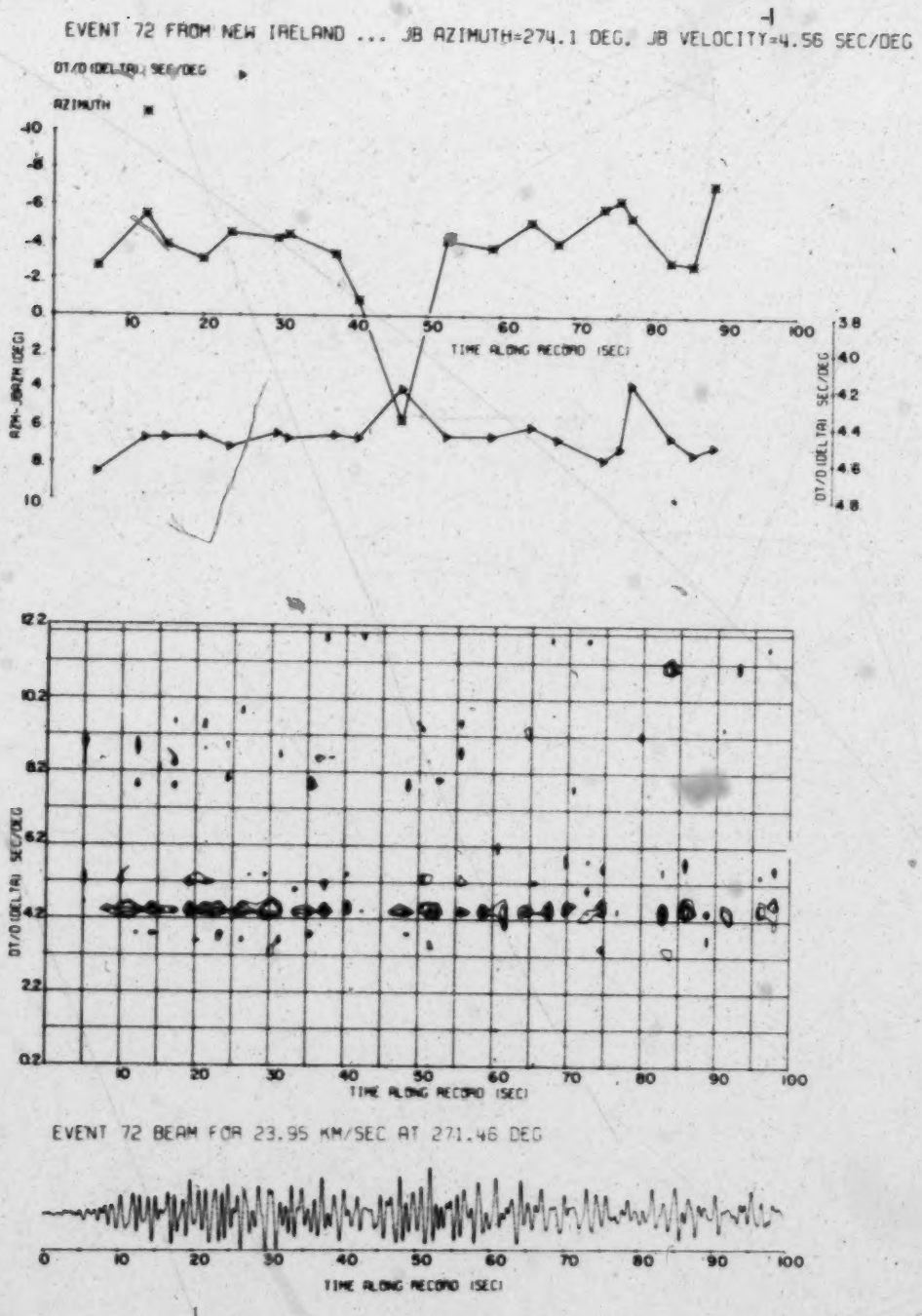
EVENT 72 FROM NEW IRELAND ... JB AZIMUTH=274.1 DEG. JB VELOCITY=4.56 SEC/DEG
DT/D (DELTA) SEC/DEG
AZIMUTH
AZM-JBAZM (DEG)
TIME ALONG RECORD (SEC)
DT/D (DELTA) SEC/DEG
EVENT 72 BEAM FOR 23.95 KM/SEC AT 271.46 DEG
TIME ALONG RECORD (SEC)

Figure 11.

Figure 12. Covespagram of event 74 from the Hindu Kush region: $\Delta$ = 92°, magnitude = 5.2, and depth = 210 km.

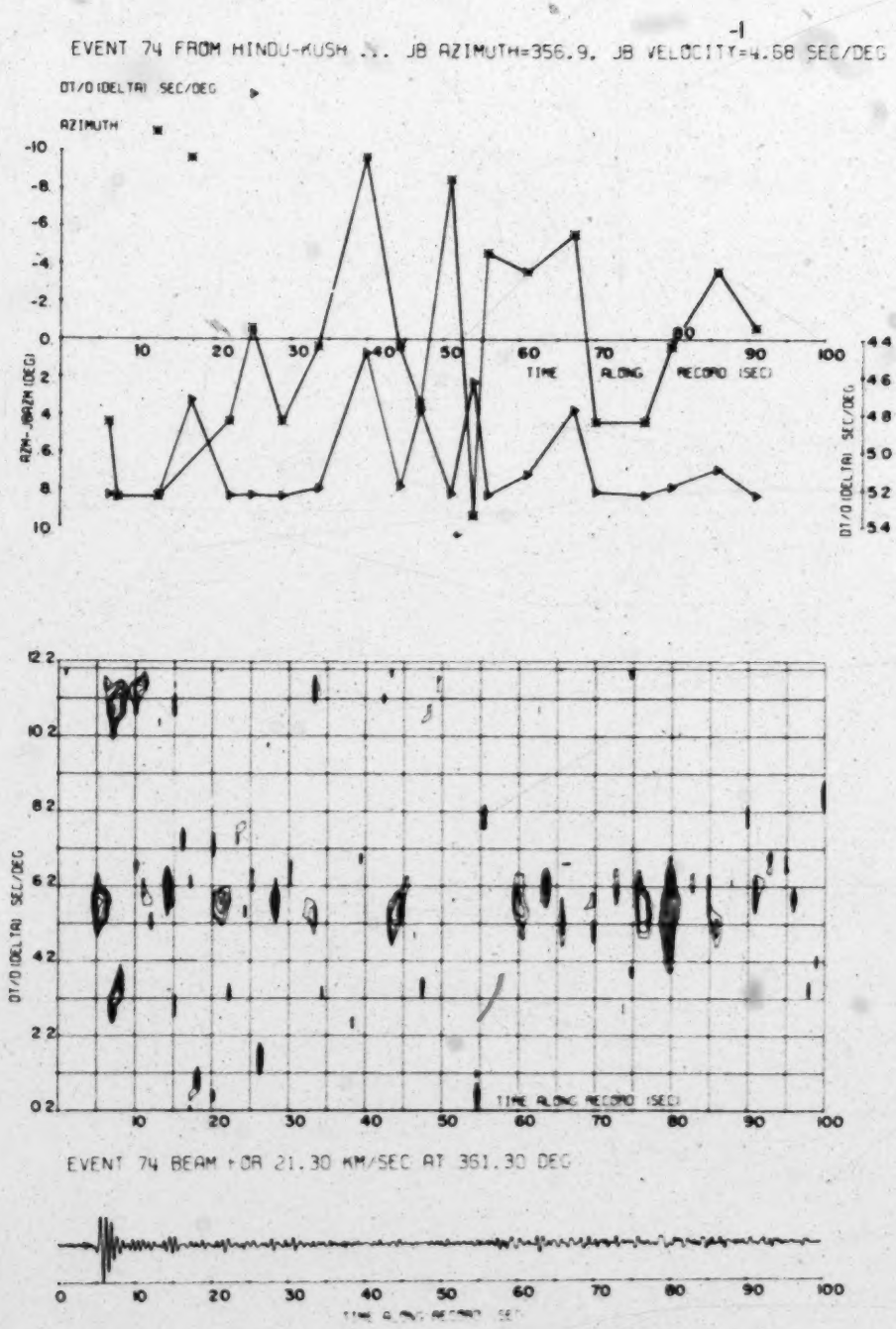
EVENT 74 FROM HINDU-KUSH ... JB AZIMUTH=356.9, JB VELOCITY=4.68 SEC/DEG
DT/D(DELTA) SEC/DEG
AZIMUTH
AZM-JBAZM(DEG)
TIME ALONG RECORD (SEC)
EVENT 74 BEAM FOR 21.30 KM/SEC AT 351.30 DEG

Figure 12.

to be typical of nearly all events from the Asian region.

In addition to these examples a number of events from the Aleutians, Japan, and South America were analyzed by the Covespa process, and revealed very little trailing energy in the P coda with the exception of one event from Japan (magnitude 6.1) which indicated a moderate manifestation of this phenomenon comparable to event 88 (magnitude 5.2) in the definition of the coherency contours.

## 4. Interpretation

The first modern seismic investigations of upper mantle discontinuities were done by Gutenberg (1960), who noticed that PP, pP', and pPP phases (the primed P denotes a ray that has passed once through the interior of the earth, including the core, from the source to the receiver) have more or less emergent beginnings which arrive early and are probably due to reflections from the Moho or other discontinuities beneath the earth's surface. Subsequently, Hoffman, Berg, and Cook (1961) using information derived from the reflection of energy from large quarry blasts claimed to have discovered evidence for discontinuities at 190, 520, and 910 km. Anderson and Toksöz (1963) studied surface waves and

found that there does in fact exist a low velocity channel, as indicated by models CIT 8 and 9 for the New Guinea - Pasadena data, bounded on the top by a gradual decrease in velocity commencing at a depth of about 50 km and on the bottom by a sharper increase in velocity at about 150 km, the region within being formed by the existence of a small amount of partial melt in the upper mantle material (Anderson and Sammis, 1970). The investigation of upper mantle structure using body wave phases has also been done by Archambeau, Flinn, and Lambert (1969) who employed spectral amplitudes and travel times to discover that abnormally low velocities exist within a region extending from approximately the base of the crust to a depth of about 150 km. Experimental observations of P'P' and its precursors as an indication of upper mantle structure were done by Adams (1968), by Engdahl and Flinn (1969), and by Bolt, O'Neill, and Qamar (1969). Adams has discovered world-wide reflections at a depth of 65 - 70 km and regional reflections at depths of 110 - 140 km (Siberia) and 159 - 190 km (Western Europe). More recent work employing this method has been done by Whitcomb and Anderson (1970) and Whitcomb (1971, 1973) who have found, among other discontinuities, strong reflections at 50 km, at 130 km and at 630 km.

In light of these investigations on upper mantle discontinuities it seems natural to associate the observed repetitive energy groupings seen in the Covespagrams as being due to reflection, single or multiple, from such velocity transition zones. However, the energy pattern which is nearly constant within each group must be interpreted on the basis of the source function, pP, sP, and any reverberations within the crust. From the time duration of such groups it may be possible to derive some information concerning the size of these sources. Assuming a shallow seismic disturbance propagating at a velocity of 2 or 3 km/sec and that a coherent group is typically 20- 30 seconds in duration, the source length should be less than 40-60 km for magnitudes of 5.1 to 6.0. This estimate is comparable with observations of surface rupture length of many shallow earthquakes (Bonilla, Figure 3.16, 1970).

It has been established that for the observed events each energy group is of 20 to 30 seconds in extent and that the period of repetitions is in the range 35 to 45 seconds. With the exception of event 74 (figure 12), these events are all situated at shallow depths ($h < 33$ km, where 33 km is often referred to as "normal depth") and it is a straightforward matter to investigate the theoretical time differences by modelling using the phase pdpP proposed by Davies, Kelly, and

Filson (1971). Figure 13 shows the scheme envisaged where the phase pdpP is a ray which travels from the source down to the discontinuity at depth d, is reflected upward to the surface (which is a strong reflector), and then is reflected again, travelling on to the receiver. The time differences between arrivals for such rays and direct P at a distance of 89° has been calculated and is summarized in table 1, which is for surface focus earthquakes. The variation in the time differences between surface focus and normal depth earthquakes was generally less than 0.01 sec. The model used for these results is the Birch-Wiggins lower mantle velocity model coupled with the University of Alberta, UA4, upper mantle profile.

In keeping with the average observed periods of repetition for the energy groups the discontinuity at 150 km seems most preferable. However, it must be emphasized that this is only an average since a small number of events does not permit regionalization of the discontinuity depths. It appears, though, from the variation of the periods that there is a strong reflector of energy in the depth range 130 km to 170 km corresponding to the sharp increase in velocity at the bottom of the low velocity channel. The burst of energy which was observed beginning at about 140 sec after the initial P arrival and was visible on both the Covespagram

Figure 13. Ray plot showing the proposed phase pdpP for d = 150 km at a distance of 89°.

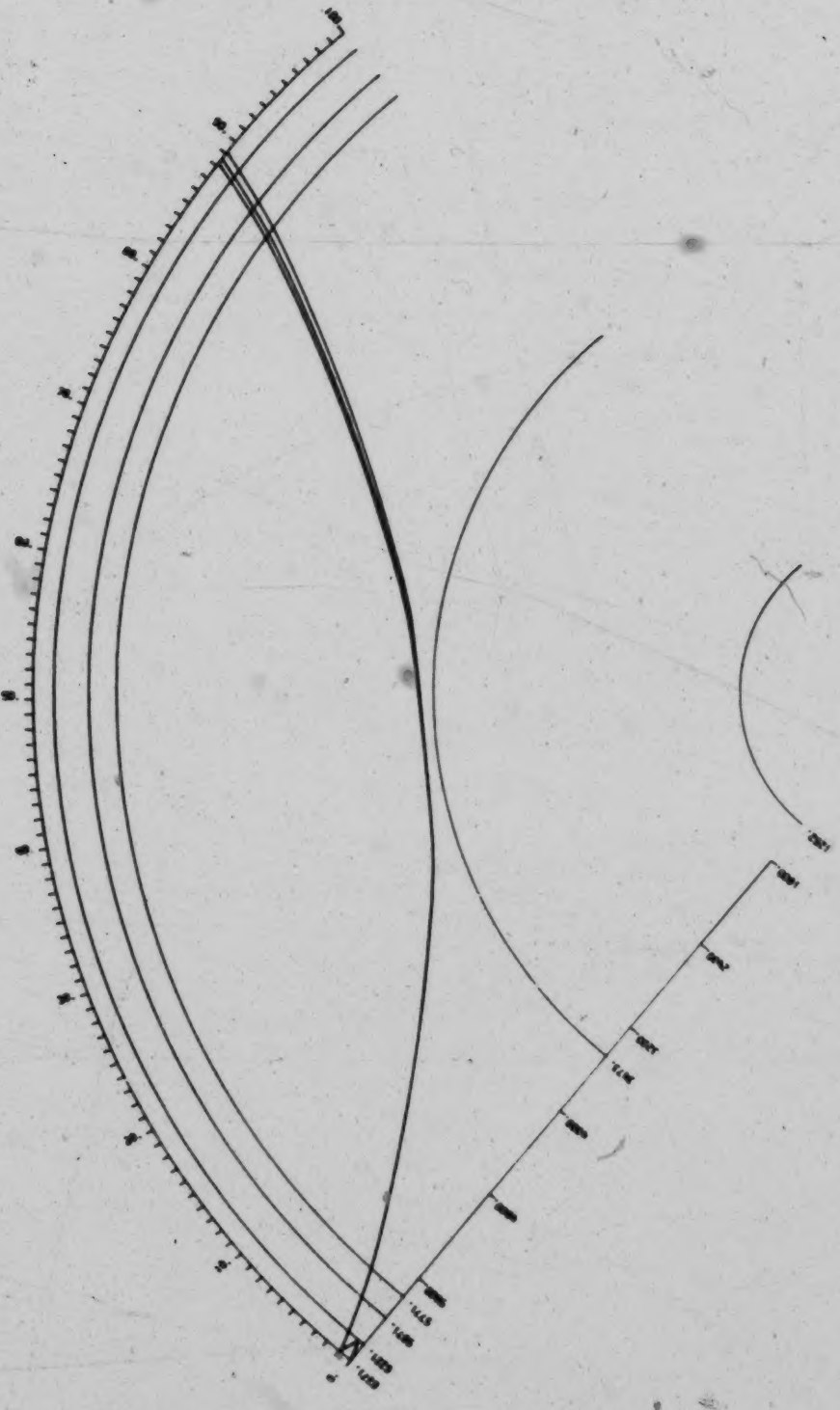


Figure 13.

Table 1. The time differences between the phase pdpP and the direct P arrivals for various depths of discontinuity, d, are shown for surface focus earthquakes.

| Depth of Discontinuity (km) | Time Difference (pdpP-P) (sec) |
|---|---|
| d = 720 | 152 |
| d = 700 | 149 |
| d = 650 | 141 |
| d = 600 | 132 |
| d = 500 | 114 |
| d = 400 | 93 |
| d = 300 | 70 |
| d = 150 | 37 |
| d = 100 | 27 |

and the summed trace (figure 9), may be indicative of p650pP. Slight variations in dip between successive multiple reflectors probably cause the velocity and azimuth variations which begin by being relatively constant and then assume more pronounced deviations. The immediate and strong variations in velocity and azimuth of the arrivals from event 74 (figure 12) indicate the structural complexity of the Asian region in general. Questions concerning the location of the reverberations, whether beneath the source or receiver, cannot yet be satisfactorily answered and may prove to be a combination of the two. This may only be resolved by the inclusion of a large amount of data from earthquakes of varying magnitudes, depths, azimuths, and distances.

## 5. Conclusion

The Covespa process used here presents a clear picture of the seismic arrivals in azimuth, slowness, and time. It is particularly useful in examining teleseismic events which have well developed P coda for the purpose of extracting information concerning the earthquake source and upper mantle structure. This method seems applicable for most earthquakes of magnitude greater than 5.1 whereas the P'P' precursor method requires earthquakes of magnitude 6.0 or greater. Therefore, far better spatial distribution of events

in relation to regions of tectonic activity may now prove to be available for the study of upper mantle structure.

# CHAPTER III

# SEISMIC ARRAY EVIDENCE FOR A LOWER MANTLE HETEROGENEITY BENEATH THE ISLAND OF HAWAII

## 1. Introduction

In this chapter the detection of the first arrivals of body waves by the seismic array (VASA) and the determination of the wave parameter $p = dT/d\Delta$ will be discussed. Two of the methods used to calculate the wave slowness involve the inversion of the relative arrival times of the body phases at the individual sensors of the array, and the third method involving the application of coherency techniques to the P coda of array data has essentially been discussed in the preceding chapter.

The results of the $dT/d\Delta$ measurements will then be discussed in the context of the earth's mantle velocity structure in general, and the structure near the base of the mantle underlying the geologically and geophysically interesting Hawaiian islands (Chapter IV) in particular. The ability of an array possessing three or more sensors to independently determine both the apparent velocity (inverse slowness) and the true azimuth of an arriving phase will be used in a detailed study of the behavior of body waves passing through this region.

## 2. Array Determined dT/dΔ Methods and dT/dΔ Observational Results

In 1970 the VASA array in central Alberta recorded approximately 100 events, eight being from the Tonga and Samoa islands region. Additionally the Peace array and stations FSJ, MCC, and EDM recorded a total of 32 Tonga earthquakes from 1969 to 1971 having good signal-to-noise characteristics and magnitudes greater than 5.3. This comprised the raw data set.

dT/dΔ calculations from the VASA digital data were carried out using three methods. The first two methods both involved first arrival phase time determinations by a semiautomatic technique employing the cross-correlation of approximately the first cycle and a half of the initial P arrival for all station pairs. Since all station pairs produced redundant time differences this permitted checks to be made on the data scatter. For the critical South Pacific events the length of the data string to be cross-correlated and its position along the record were varied somewhat and the correlation procedure was repeated thus providing a check on the stability of the time determinations. Time determinations were also made by hand for all events.

The first method of inverting the time differences to velocities and azimuths was the direct three-station

inversion. The array was first broken down into all combinations of three stations and the following analysis was performed on each triangle.

Let the station triangle be as shown in figure 14. The velocity along leg 1,2 is

$$C_{12} = \Delta_{12}/T_{12} \qquad (3\text{-}1)$$

where $\Delta_{12}$ is the distance from station 1 to station 2 and $T_{12}$ is the time difference between the wavefront arrivals at the two stations. Similarly for leg 1,3 one has

$$C_{13} = \Delta_{13}/T_{13} \qquad (3\text{-}2)$$

Then the apparent velocity of the wavefront will be given by

$$C = C_{12} \sin A \qquad (3\text{-}3)$$

and also

$$C = C_{13} \sin(A + \alpha) \qquad (3\text{-}4)$$

where A is the angle formed by leg 1,2 and the wavefront and $\alpha$ is given by the known triangle geometry (angle 213). Solving (3-3) and (3-4) for C one has

$$\tan A = \sin A/\cos A$$

$$= \sin \alpha/(C_{12}/C_{13} - \cos \alpha) \qquad (3\text{-}5)$$

giving

Figure 14. The three station velocity and azimuth determination. The array geometry is given by angle $\alpha$ and distances $\Delta_{12}$ and $\Delta_{13}$. The wavefront enters the array at station 1 with velocity C, making an angle, A, with the side (12). $C_{12}$ and $C_{13}$ are the projections of C along legs (12) and (13).

# THREE STATION VELOCITY-AZIMUTH DETERMINATION

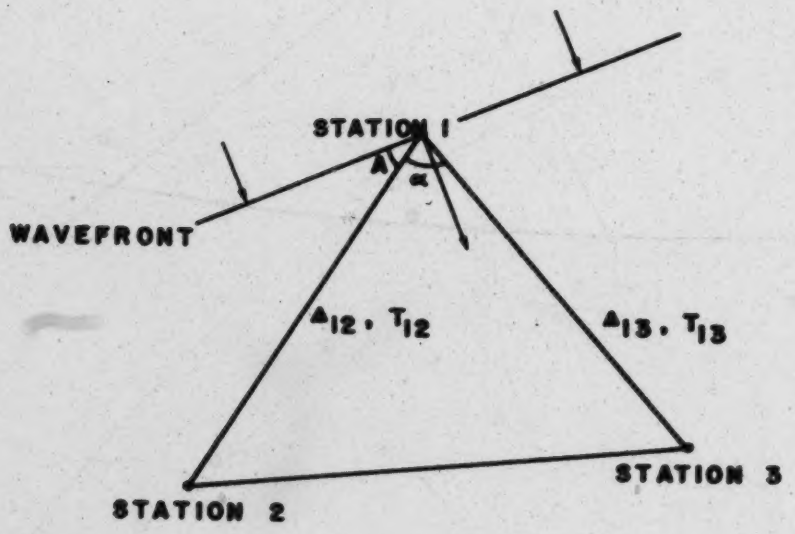


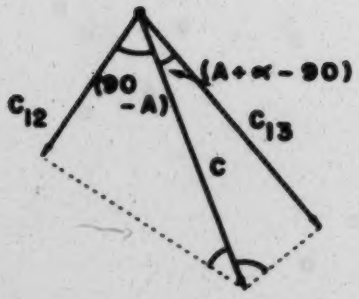


$C_{12} = \cos(90-A) = \sin(A)$

$C_{13} = \cos(A+\alpha-90) = \sin(A)$

Figure 14.

$$A = \tan^{-1}[\sin \alpha/(C_{12}/C_{13} - \cos \alpha)] \qquad (3\text{-}6) \quad .$$

Hence C may be found using equation (3-3).

Thus the azimuth and the apparent velocity may be found for station 1. This is then repeated for all such triangles. The individual velocities and azimuths are weighted according to the relative area of their respective triangles. The weighted velocities are then averaged and the weighted azimuths are transformed to a common point (e.g. the center of the array) and then averaged.

The second technique involves a least square method for direct measurement of $dT/d\Delta$ and is described by Husebye (1969). A brief outline of the method will be presented here.

Let

$$T = B_1 z_1 + B_2 z_2 + \ldots + B_k z_k \qquad (3\text{-}7)$$

represent the response surface of the relative arrival time over an arbitrary array. The $\{B_i\}$ are coefficients to be determined by a least squares fitting of the surface to the data and the $\{z_i\}$ are defined as follows:

$$z_1 \equiv 1.0 \ , \quad z_2 = \phi^{A1} \ , \quad z_3 = \lambda^{A2} \ , \quad z_4 = \phi^{2A1} \ , \ \ldots \qquad (3\text{-}8) \ .$$

The $\{z_i\}$ are the transformed coordinates of the array station locations $\phi$ (latitude) and $\lambda$ (longitude) and the

exponents A1 and A2 are to be determined by a first order expansion of the fitted surface T about the first guesses of A1, A2.

Since T is the fitted surface determined from the guesses (initially A1 = 1.0, A2 = 1.0) expanding about A1,A2 to first order gives

$$T_{ob} = T + (A1-1.0)\ \frac{\partial T}{\partial A1} + (A2-1.0)\ \frac{\partial T}{\partial A2} \qquad (3\text{-}9)$$

or

$$T_{ob} = T + (A1-1.0)\ \frac{\partial T}{\partial \phi}\phi \ln\phi + (A2-1.0)\ \frac{\partial T}{\partial \lambda}\lambda \ln\lambda \qquad (3\text{-}10)$$

where $T_{ob}$ are the expected values of the arrival times. Equation (3-10) is now treated as a new surface given by

$$T = B_1 z_1 + B_2 z_2 + \ldots + B_k z_k + (A1-1.0)\, z_{k+1} + (A2-1.0)\, z_{k+2} \qquad (3\text{-}11)$$

where

$$z_{k+1} = \frac{\partial \bar{T}}{\partial \phi}\ \phi \ln \phi \qquad (3\text{-}12)$$

and

$$z_{k+2} = \frac{\partial \bar{T}}{\partial \lambda}\ \lambda \ln \lambda \qquad (3\text{-}13)$$

The approximate values $\partial\bar{T}/\partial\phi$ and $\partial\bar{T}/\partial\lambda$ are determined by differentiating the fitted response surface T given by (3-7). Now, a new surface is formed in the manner of (3-7):

$$T = B_1 z_1 + B_2 z_2 + \ldots + B_k z_k + B_{k+1} z_{k+1} + B_{k+2} z_{k+2} \qquad (3\text{-}14)$$

where $B_{k+1}$ = A1-1.0 and $B_{k+2}$ = A2-1.0. This new response surface is fitted in a least squares fashion to the data giving values for $B_{k+1}$ and $B_{k+2}$ from which are derived the new values for A1 and A2,

$$A1 = B_{k+1} + 1.0 \quad , \qquad (3\text{-}15)$$

$$A2 = B_{k+2} + 1.0 \quad , \qquad (3\text{-}16)$$

which are used in place of the first guesses in a new iteration. The iterations are repeated until either certain preset error criteria are satisfied or until no further improvement occurs. For the VASA array the response surface

$$T = 1.0 + B_2 \phi^{A1} + B_3 \lambda^{A2} + B_4 \phi^{A1} \lambda^{A2} \qquad (3\text{-}17)$$

proved satisfactory requiring only a single iteration to reach a stable solution. Large arrays possessing apertures greater than 3° will require a response surface of second order in $\phi$ and $\lambda$:

$$T = 1.0 + B_2 \phi^{A1} + B_3 \lambda^{A2} + B_4 \phi^{A1} \lambda^{A2} + B_5 \phi^{2A1} + B_6 \lambda^{2A2} \ldots \qquad (3\text{-}18) .$$

An array similar to Husebye's (1969) with an aperture of 10° and fifteen randomly placed sensors was tested

using (3-18) and required two iterations to reach a stable solution.

The apparent slowness is determined by finding the orthogonal components for each station i, $\partial T/\partial \phi_i$ and $\partial T/\partial \lambda_i$, in the north and east directions respectively using the best fitting time response surface, T. The resultant slowness $p_i$ is given by

$$p_i = \sqrt{u_i^2 + v_i^2} \qquad (3\text{-}19)$$

where $u_i = \frac{\partial T}{\partial \phi_i} \hat{e}_\phi$ and $v_i = \frac{\partial T}{\partial \lambda_i} \hat{e}_\lambda$,

$\hat{e}_\phi$ and $\hat{e}_\lambda$ being unit vectors pointing north and east respectively.

The azimuth is found using the equation

$$\tan \gamma_i = v_i/u_i \qquad (3\text{-}20)$$

In a similar manner $d^2T/d\Delta^2$ may also be found. These quantities need not be calculated at the station locations but, in general, can be determined for any set of points within the array.

Errors are determined by assuming that errors in the various parameters ($u_i$, $v_i$, $p_i$, $\gamma_i$, ...) are independent Gaussian variables having zero mean and then finding the first order perturbations on the parameters (Husebye, 1969). Computationally the problem is set up in the form of normal linear equations and solved using

matrix operations: from equation (3-7) with k = 4 the normal equations will be

$$\Sigma z_1 T = \Sigma z_1 z_1 + B_2 \Sigma z_1 z_2 + B_3 \Sigma z_1 z_3 + B_4 \Sigma z_1 z_4$$

$$\Sigma z_2 T = \Sigma z_2 z_1 + B_2 \Sigma z_2 z_2 + B_3 \Sigma z_2 z_3 + B_4 \Sigma z_2 z_4$$

$$\Sigma z_3 T = \Sigma z_3 z_1 + B_2 \Sigma z_3 z_2 + B_3 \Sigma z_3 z_3 + B_4 \Sigma z_3 z_4$$

$$\Sigma z_4 T = \Sigma z_4 z_1 + B_2 \Sigma z_4 z_2 + B_3 \Sigma z_4 z_3 + B_4 \Sigma z_4 z_4 \qquad (3\text{-}21)$$

where the $z_i$ are defined by (3-8) and the summation runs over all points of observation. (3-21) can be put into matrix form:

$$C = B.Z \qquad (3\text{-}22)$$

where C is the column vector whose elements are the left side of (3-21) and B is the column vector formed by the coefficients $\{B_i\}$ and Z is the matrix formed by the summation products of the $\{z_i\}$. The desired coefficients $\{B_i\}$ can be found by solving (3-22):

$$B = C.Z^{-1} \qquad (3\text{-}23)$$

The third technique of velocity-azimuth determination involves the nonlinear array processor employing a coherency measure requiring only the array geometry and

the block start times. This method was discussed in Chapter II.

$dT/d\Delta$ results for the three methods proved to be in close agreement being within 0.01 sec/deg for those events for which comparison was made (the South Pacific and Asian events). Also, it was observed that the hand picked first arrival times yielded velocities and azimuths that were very nearly the same as those obtained using the cross-correlation techniques although with the latter methods the data scatter was considerably reduced and for this reason was deemed superior.

The intrinsic accuracy of the results is ±0.2 km/sec if one considers errors in determining the first arrival time of the wavefront at the stations of the array and the variations in the azimuth of the wavefront.

The data from the individual Peace stations were combined with station FSJ and averaged after $dT/d\Delta$ computation and the same operation without averaging was applied to data from stations MCC and EDM.

Figure 15 shows one particular record suite. Figure 16 displays the results from VASA in the teleseismic distance range 20° to 100° with the solid curve representing the apparent slowness as determined from the tables of Jeffreys and Bullen (1958) by cubic spline fitting and differentiation. The epicentral distances have all been corrected to correspond to earthquakes

Figure 15. The vertical component of initial ground motion for the Tonga event of July 28, 1970, at 04 h 47 m and 47.7 s UT as recorded by stations of the VASA array. The WWVB signal and indicating second marks are shown with each seismogram. The magnitude was 5.2, and the depth was normal (33 km).

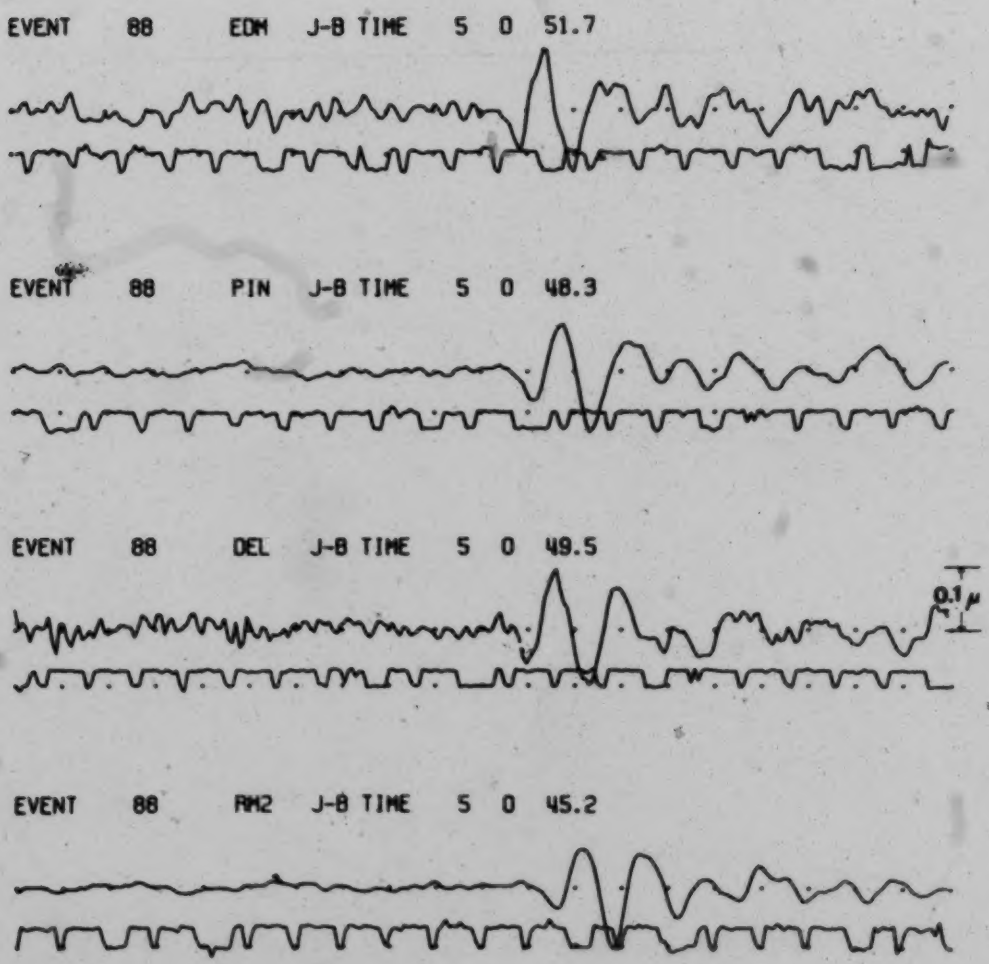
EVENT 88 EDM J-B TIME 5 0 51.7
EVENT 88 PIN J-B TIME 5 0 48.3
EVENT 88 DEL J-B TIME 5 0 49.5
0.1 μ
EVENT 88 RM2 J-B TIME 5 0 45.2

Figure 15.

Figure 16. The $dT/d\Delta$ observations of initial P waves for all events between 20° and 100° as recorded from June to August 1970 by VASA. The $dT/d\Delta$ curve is obtained from the J-B tables for a normal depth source. Squares indicate events from the Aleutians and Japan; triangles, events from Tonga and Samoa; plus signs, events from South America; circles, events from Asia; crosses, special Solomon region events.

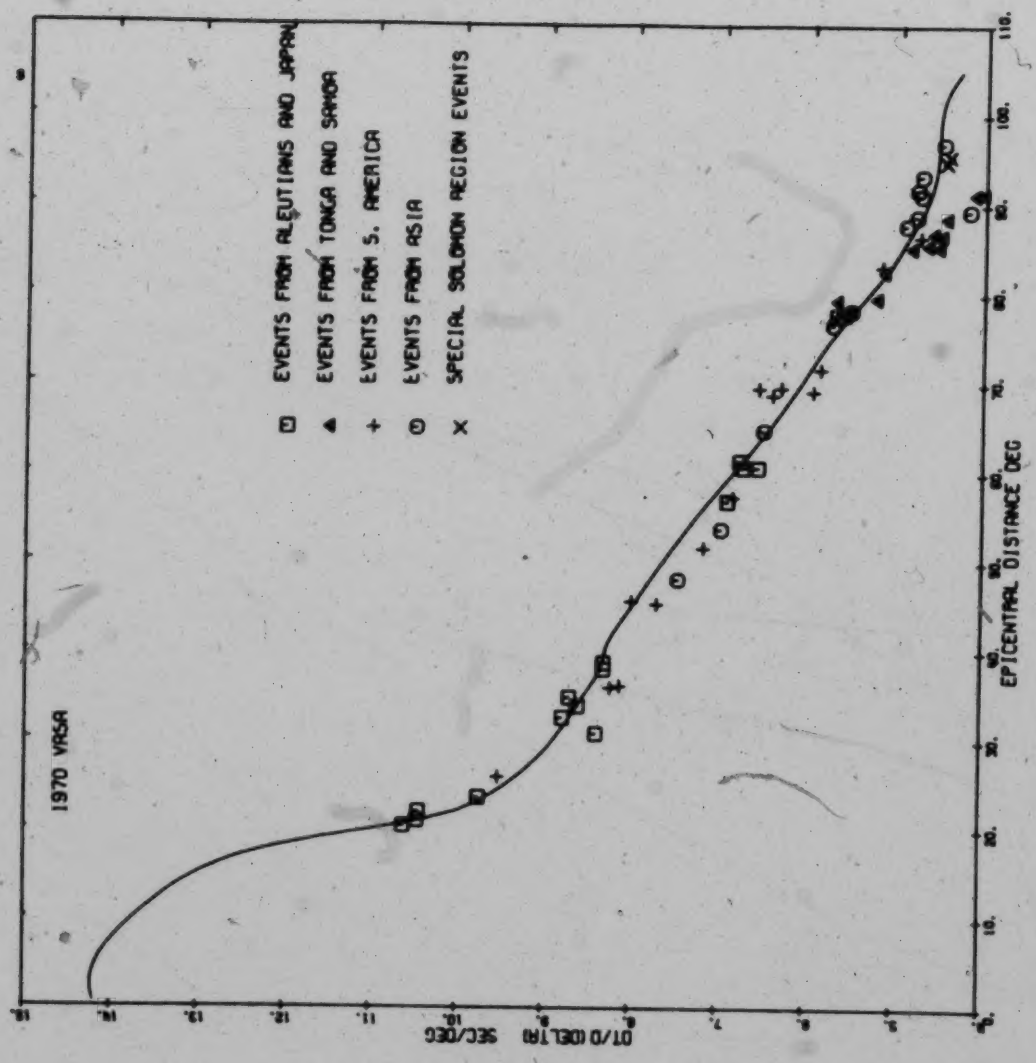
1970 VASA
EVENTS FROM ALEUTIANS AND JAPAN
EVENTS FROM TONGA AND SAMOA
EVENTS FROM S. AMERICA
EVENTS FROM ASIA
SPECIAL SOLOMON REGION EVENTS
EPICENTRAL DISTANCE DEG
DT/D DELTA SEC/DEG

Figure 16.

occurring at normal depth (33 km). As can be seen by inspection the majority of events are in agreement with the Jeffreys-Bullen (J-B) curve, some of the scatter being immediately attributable to the relatively low magnitude of some events and the fact that for some events part of the array was inoperative. Johnson (1969) has previously observed small scale $dT/d\Delta$ anomalies for different earthquake regions and such seems to be the case for some events shown here. There is, however, a striking deviation from the normal in the distance range 84° to 95° from earthquakes in the Tonga and Samoa islands region whereas events from the Solomon islands and New Ireland (angular separation from Tonga of 20° at the receiver) and Asia and South America show normal $dT/d\Delta$ results. Included in the anomalous results are one event from the Easter island region and one event from Taiwan. The anomalous results have $dT/d\Delta$ values that are low (phase velocities therefore will be high as shown in figure 17a) with a generally monotonic behavior with distance. Figures 17 b and c show the supporting results as determined by the Peace- FSJ array and the MCC-EDM station pair. Additionally through the courtesy of Dr. D. Davies, an independent analysis was made of LASA recordings for 18 events (1966-1969) in the Fiji and New Hebrides regions. The phase velocities from this study are shown in figure 18 and indicate variations from

Figure 17. Observations of phase velocity for Tonga earthquakes as recorded by (a) VASA, (b) the FSJ-Peace array, and (c) the EDM-MCC station pair. The phase velocity curves are for a lower mantle based on Birch's (1964) model 2 and its modification (d). The solid sections of the phase velocity curves are for the geometric rays, and the dashed portions are diagramatic for the wave in the high-velocity wave guide.

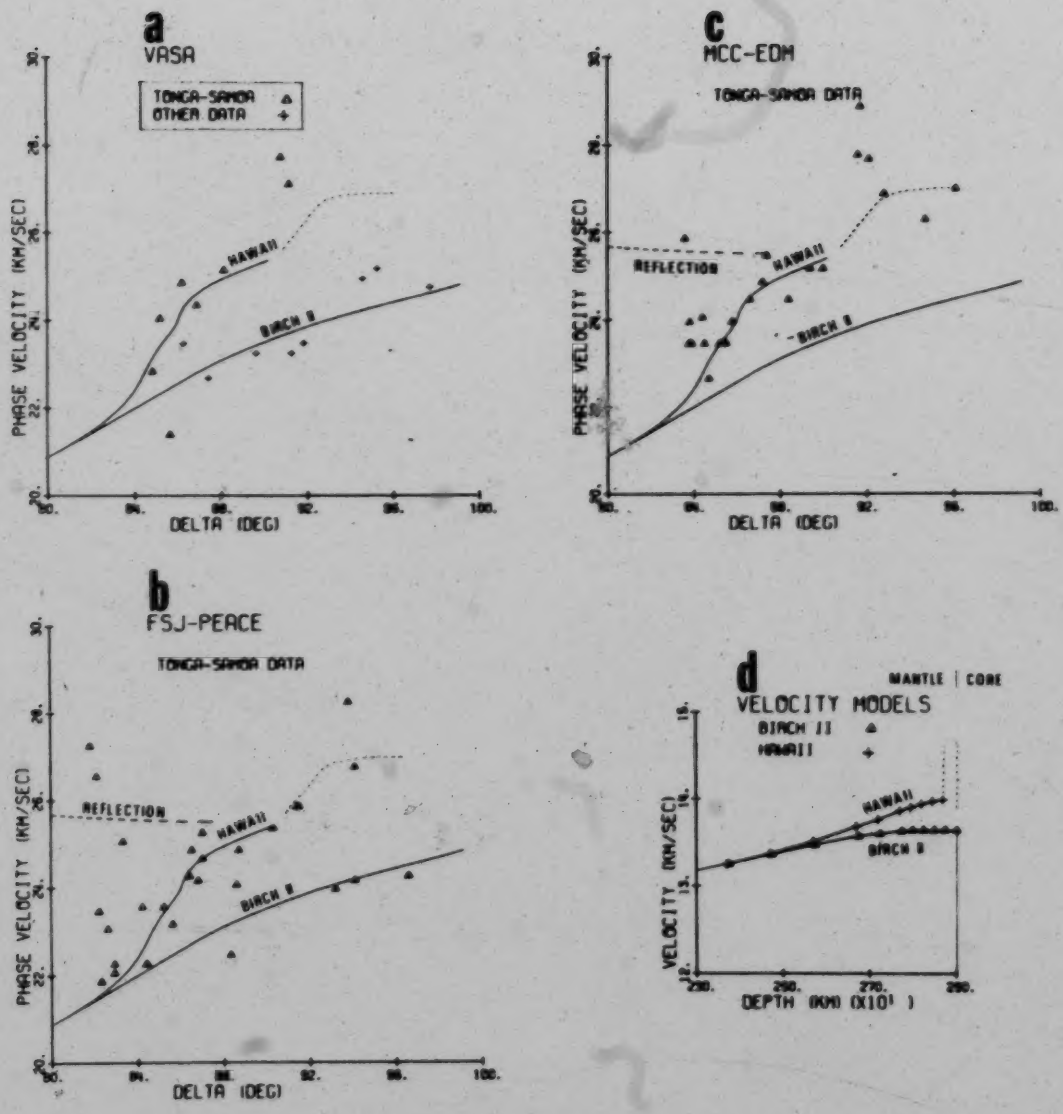
a
VASA
TONGA-SAMOA
OTHER DATA
HAWAII
BIRCH II
PHASE VELOCITY (KM/SEC)
DELTA (DEG)
c
MCC-EOM
TONGA-SAMOA DATA
REFLECTION
HAWAII
BIRCH II
PHASE VELOCITY (KM/SEC)
DELTA (DEG)
b
FSJ-PEACE
TONGA-SAMOA DATA
REFLECTION
HAWAII
BIRCH II
PHASE VELOCITY (KM/SEC)
DELTA (DEG)
d
MANTLE | CORE
VELOCITY MODELS
BIRCH II
HAWAII
HAWAII
BIRCH II
VELOCITY (KM/SEC)
DEPTH (KM) (X10¹ )

Figure 17.

Figure 18. LASA P-wave phase velocities for the distance range 91°- 100° and the azimuthal range 240°- 270° (Fiji and New Hebrides regions). The solid phase velocity curve is derived from the J-B tables.

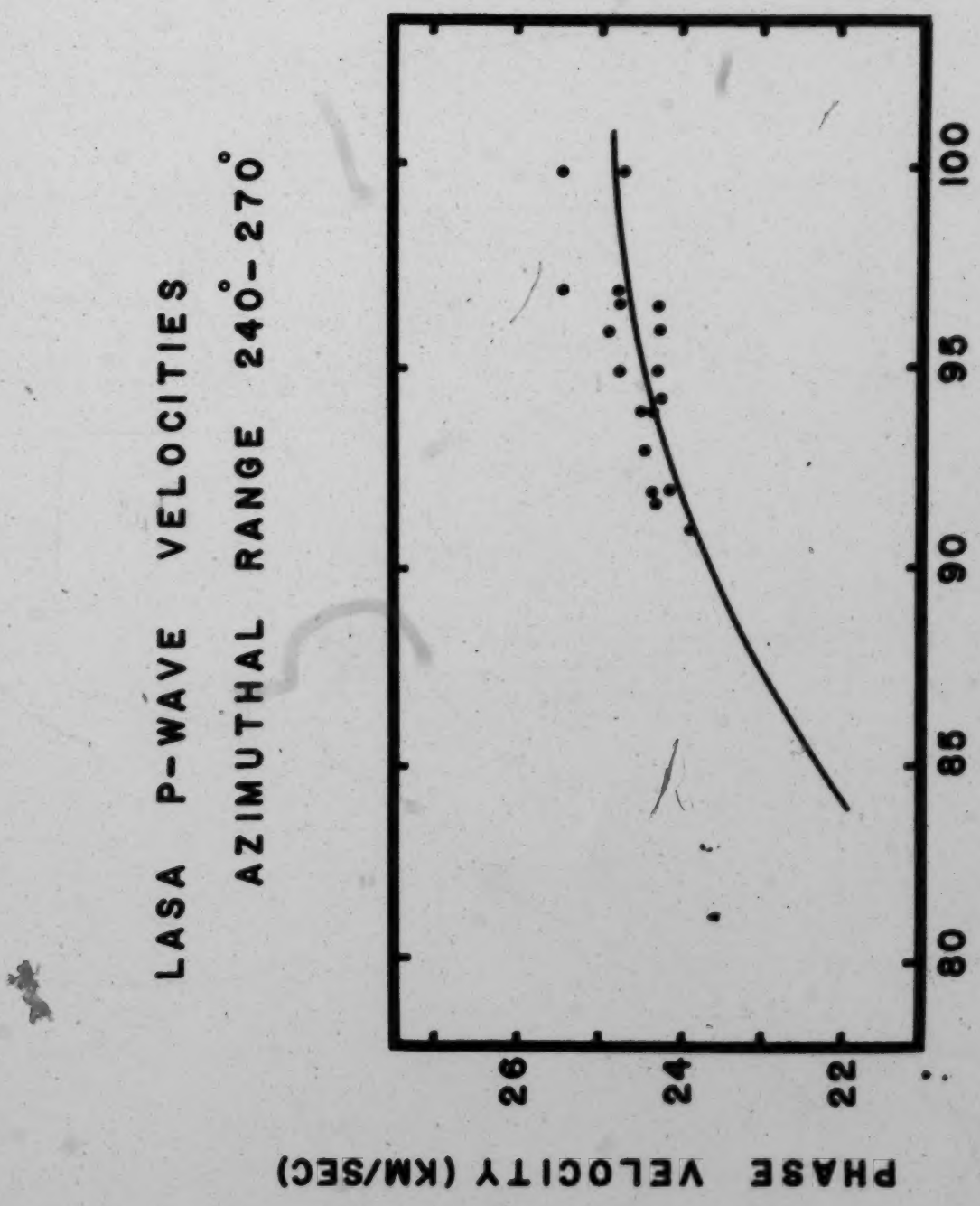
LASA P-WAVE VELOCITIES
AZIMUTHAL RANGE 240°-270°
PHASE VELOCITY (KM/SEC)
26
24
22
80
85
90
95
100
EPICENTRAL DISTANCE (DEG.)

Figure 18.

23.5 to 25.7 km/sec at epicentral distances of 91° to 100°, seven events being low with respect to the LASA baseline or J-B derived curve and 11 having slightly high phase velocities. Fourteen of the LASA events have velocity anomalies that are less than ±0.3 km/sec. Further, the azimuthal anomalies for VASA are generally less than 3° with one being 5.5° and those for LASA are generally less than ±2° with one as large as 7°. Curiously, most of the azimuthal anomalies for VASA tend to be clockwise from the geocentric azimuths to the sources whereas those for LASA tend to be in a counter clockwise sense. More will be said about this shortly.

Upon analysis of the arrival times at individual VASA stations one sees a very broad azimuthal effect with these stations differing by only $-0.2 \pm 0.7$ sec from the J-B tables (corrected for ellipticity and station elevation) when all events from epicentral distances of 30° to 95° and azimuths 0° to 360° are considered. The analysis of quadrants and individual stations is given in table 2. Since many of the events come from Benioff zones (see Sorrells et al., 1971) the azimuthal dependence will be due, in part, to source effects. As can be seen individual stations differ by only 0.1 to 0.3 sec in any single quadrant. For all events into VASA the azimuth of arrival was determined independently of

Table 2. Differences between observed travel times at VASA and the J-B tables for all earthquakes between 30° and 100° are shown.

| Station | Number of Observations | Azimuth | Time Difference (sec) | Standard Deviations (sec) |
|---|---|---|---|---|
| All stations | 187 | | -0.2 | ±0.7 |
| EDM | 53 | 0°-360° | -0.3 | ±0.7 |
| T-P-D | 90 | | -0.2 | ±0.7 |
| RM1-RM2 | 41 | | -0.3 | ±0.6 |
| All | 7 | 0°-90° | -0.6 | ±0.4 |
| All stations | 50 | | -0.7 | ±0.5 |
| EDM | 17 | | -0.7 | ±0.6 |
| T-P-D | 21 | 90°-180° | -0.7 | ±0.5 |
| RM1-RM2 | 11 | | -0.6 | ±0.4 |
| All stations | 35 | | -0.2 | ±0.6 |
| EDM | 10 | 180°-270° | -0.3 | ±0.6 |
| T-P-D | 15 | | -0.0 | ±0.6 |
| RM2 | 8 | | -0.0 | ±0.6 |
| All stations | 95 | | +0.0 | ±0.6 |
| EDM | 24 | 270°-360° | -0.1 | ±0.6 |
| T-P-D | 49 | | +0.2 | ±0.7 |
| RM1-RM2 | 19 | | -0.1 | ±0.5 |

phase velocity and in general showed only slight deviations from the great circle path. From the examination of the small time residuals between individual stations it can be stated that structural effects near the receiver cannot explain the observed anomalous $dT/d\Delta$ values at distances of 85° to 95° from Tonga. Additionally there are other events from the Pacific and Asia which deviate from the worldwide average values for $dT/d\Delta$ as represented by the J-B curve (figure 16).

Figure 17 contains the observations from the three groups of seismograph stations in western Canada with the anomalously high phase velocities being observed on all three groups in the distance range 84° to 95°. Figure 19 shows the epicenters and turning points (corrected for depth of source which varies from 30 to 673 km) for the South Pacific events with the receiver systems also shown along with some representative great circle paths. As is seen these turning points lie within a region 10° in diameter at the end of the Hawaiian ridge. Due to the location of the Peace array with respect to the Tonga-Samoa region several normal events are indicated by figure 17b as corresponding closely to the Birch 2 curve. These events have their epicenters at the southern edge of the Tonga region and since their phase velocities agree with the J-B values

Figure 19. Location of earthquakes (plus signs) and recording sites (triangles) used in this study. A few great circle paths have been drawn to show the projection of the seismic rays on the surface of the earth. The turning points of rays having anomalously high phase velocities are located by crosses. Turning points with phase velocities concordant with the J-B values are denoted by squares.

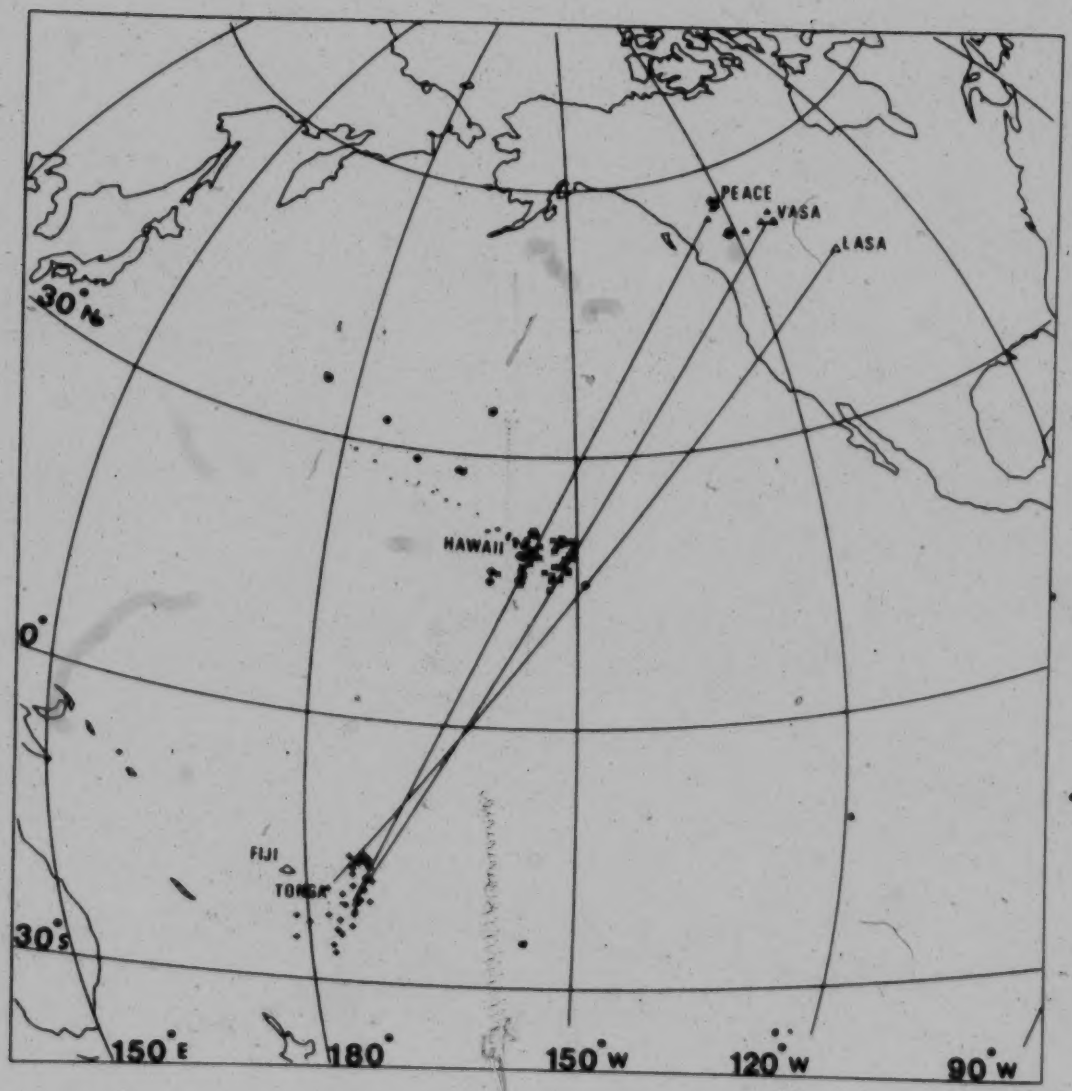
PEACE
VASA
LASA
30°N
HAWAII
0°
FIJI
TONGA
30°S
150°E
180°
150°W
120°W
90°W

Figure 19.

their turning points (squares in figure 19) appear to define the western limit of the anomalous region. In addition a single event having a normal phase velocity from Fiji into the LASA array has been reported by Iyer and Healy (1972) and it has its turning point plotted in figure 19. It seems to set a limit on the eastern edge of the anomalous region.

An expansion of this region is shown in figure 20. The data used in this diagram are the Tonga-Samoa VASA data and the Fiji-New Hebrides LASA data as they include both phase velocity and azimuth information. The diagram shows both the geocentric turning points of the ray (closed circles for LASA and open circles for VASA) and the turning points determined by taking the observed azimuth of the arriving wavefront and then extrapolating back along this ray to the halfway point (indicated by the arrowheads). The numbers at the arrowheads refer to the actual phase velocity anomaly (in km/sec above the J-B values for a particular ray) associated with that scattering point. In general when plotting the actual turning points those for VASA tend to move to the northwest and those for LASA tend to migrate to the southeast, thus separating from one another. Further, it must be remembered that for these events the distances to LASA average 93° whereas for VASA they average 89° and hence

Figure 20. Contour diagram of anomalous (observed-J-B) phase velocities for earthquakes in the South Pacific as recorded by LASA and VASA arrays. The tails of the arrows (solid circles for LASA and open circles for VASA) represent the geocentric locations of the turning points on great circle paths between the source and receiver. The arrowheads represent the actual turning points based on the observed azimuthal deviations. A map of the Hawaiian Islands is projected to the level of the turning points which are just above the core-mantle interface.

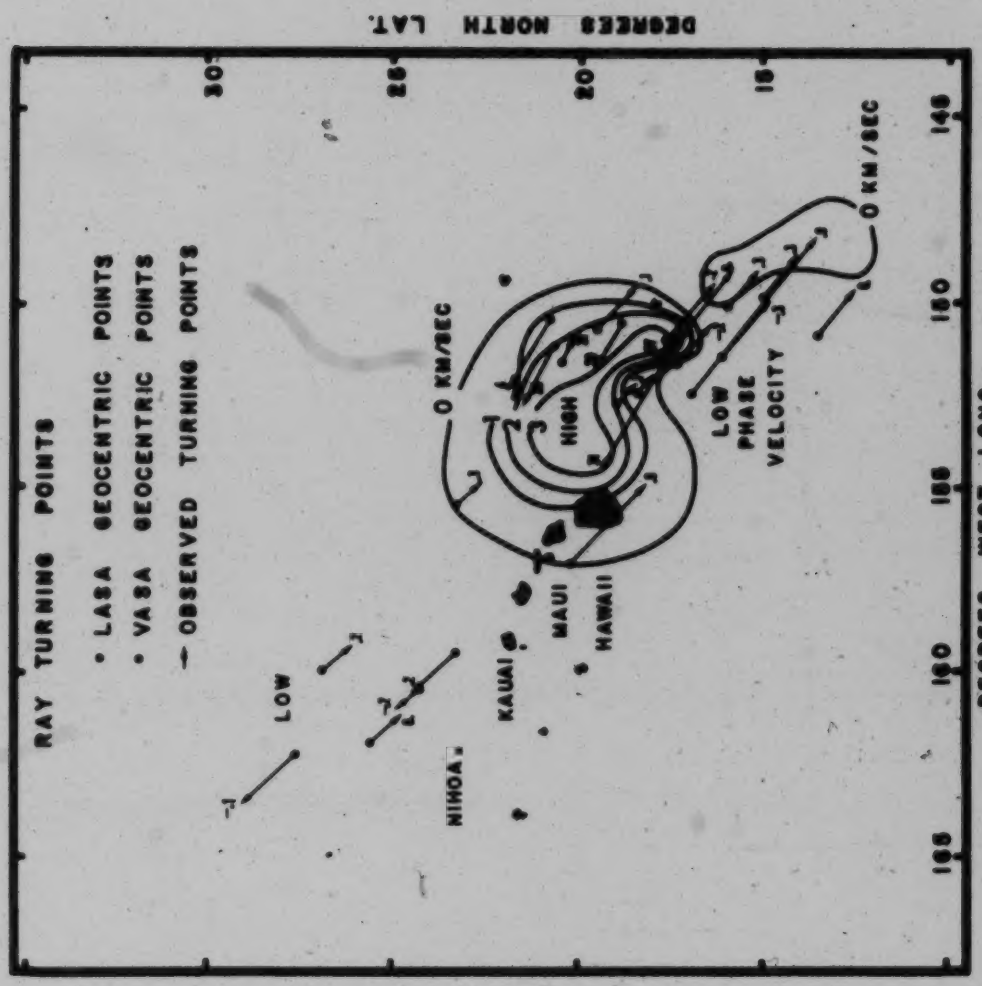
RAY TURNING POINTS
• LASA GEOCENTRIC POINTS
• VASA GEOCENTRIC POINTS
— OBSERVED TURNING POINTS
DEGREES NORTH LAT.
30
25
20
15
DEGREES WEST LONG.
165
170
175
180
185
0 KM/SEC
0 KM/SEC
LOW PHASE VELOCITY
HIGH
LOW
NIHOA
KAUAI
MAUI
HAWAII

Figure 20.

the rays to LASA will generally bottom as much as 100 km below those to VASA. Therefore, thinking three dimensionally the two arrays are sampling different regions at the ray turning points. The contours are drawn for illustrative purposes to help discern the patterns in phase velocity distribution: one has a central region of high phase velocity (containing points with anomalous velocities as high as 3.7 km/sec) centered just northwest of the island of Hawaii which becomes more and more normal as one moves outward from this region until normal or below normal phase velocities are encountered.

Additional evidence of anomalously high phase velocities in this region is furnished by the S-wave arrivals. The velocities for the S wave phases were determined by the cross-correlation and manual methods and also by the coherency method which was discussed in Chapter II. The velocities into the VASA array from the Tonga islands region are plotted in figure 21 with the solid curve representing the J-B derived phase velocities for S waves. Behavior of the S phase velocities with distance seems to follow the behavior of the P wave counterparts for the available common events.

Three critical areas may be examined for the source of the anomalous $dT/d\Delta$ results: (1) source effects, in particular the location of the hypocenter on a

Figure 21. Observations of S-wave phase velocities. The open circles are due to earthquakes in the Tonga region (P-wave anomalous) and the crosses are due to events from Asia and from the Solomon Islands (P-wave normal). The solid phase velocity curve is from the J-B tables of S arrivals.

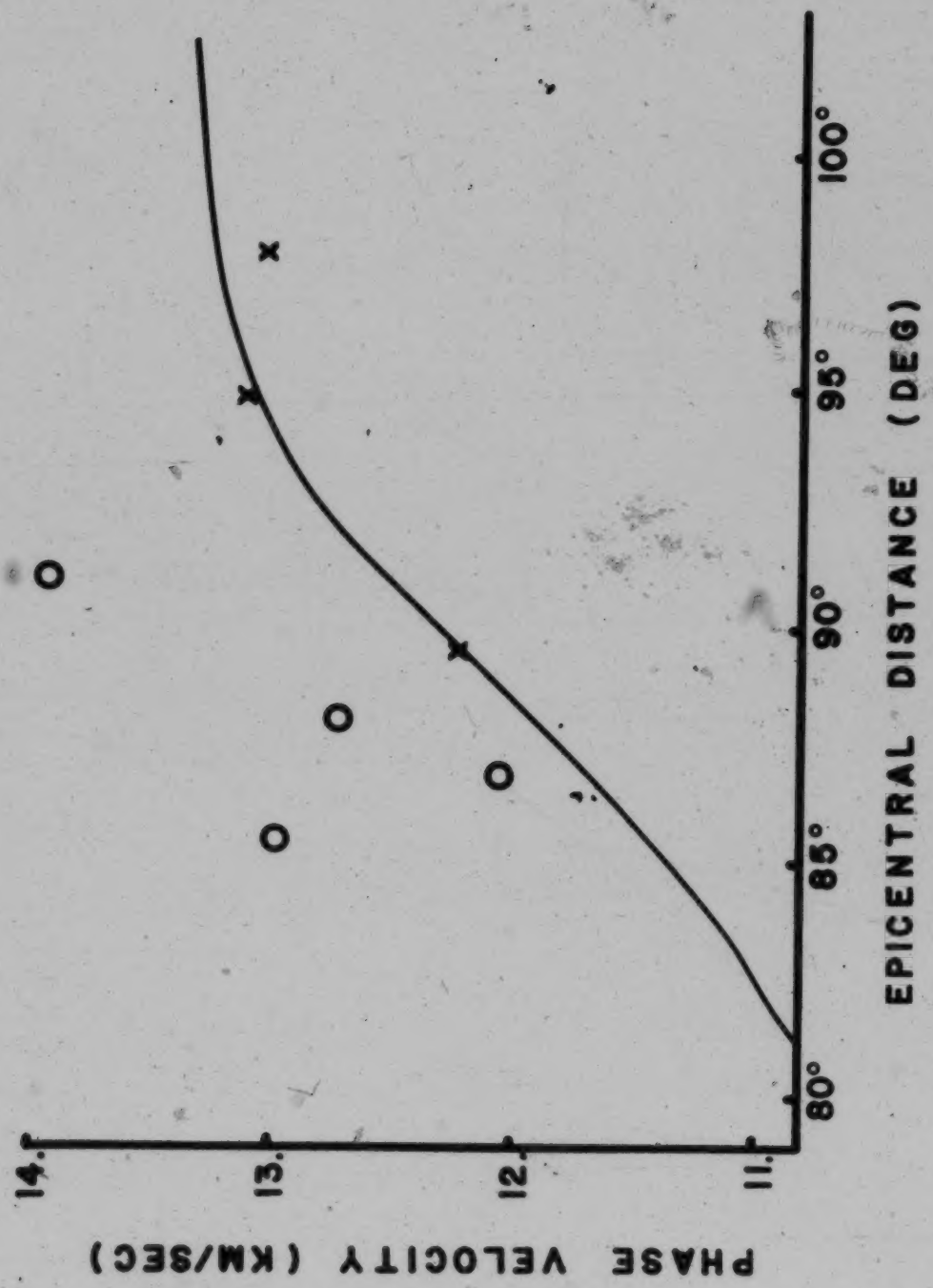
PHASE VELOCITY (KM/SEC)
14.
13.
12.
11.
EPICENTRAL DISTANCE (DEG)
80°
85°
90°
95°
100°

Figure 21.

descending plate of lithosphere in the vicinity of the Tonga islands (Isacks et al., 1968); (2) effects beneath the receiver arrays in western Canada; and (3) the vicinity of the turning point of the rays, in this case the lower mantle beneath the island of Hawaii.

Although source or receiver effects cannot be completely eliminated as contributors to the anomalous phase velocities there are several observations one can make which cast doubt on the possibility that these effects are very important. The theoretical P wave residual field due to a thick slab of relatively high-velocity material dipping steeply into the mantle has been analysed by Sorrells et al. (1971). These residuals vary too slowly with azimuth and the change with distance is too low by one or two orders of magnitude to account for the anomaly. To generate the required phase velocity anomaly one could set up a lateral velocity gradient in such a downgoing slab. Since rays into VASA at a distance of 90° are separated by only 5 minutes of arc they will be merely 0.4 km apart at 100 km from the source. In order to produce the anomaly over an array 150 km on a side one would require that two nearly parallel rays travel in two separate velocity structures separated by no more than 0.4 km so that the faster ray would gain almost 0.5 sec relative to the slower one

($\Delta = 90°$). Such a rough calculation shows that the lateral velocity gradient would have to be greater than 1 km/sec per kilometer. This concept is so unlikely both from a ray and a wave view point that source effects must be dismissed altogether.

The observed phenomenon can be mimicked by a dip of 7° to the southwest (the direction of Tonga) on the M discontinuity beneath all stations of the arrays but this is at variance with $dT/d\Delta$ from the other quadrants as displayed in figures 16 and 17. The effect of the dip should be to force increases in phase velocities from events in the direction of dip and decreases in phase velocities from events in the reverse direction. Since many events that appear normal velocitywise are not only from the directions nearly opposite to the dip but are from regions separated from anomalous events by at most 20° in azimuth at the receivers, the dipping Moho hypothesis must be discarded. Anomalous structures can be placed anywhere along the ascending or descending arms of the ray but then one requires rather large structures in the mesosphere which would lend themselves to previous detection. Variations in $dT/d\Delta$ are most easily generated at the ray turning point and therefore the anomalous velocities will be interpreted on the basis that they arise from this region in the lower mantle.

## 3. Interpretation

If, now one assumes that the region about the turning point of the ray is the most likely location of the $dT/d\Delta$ anomalies observed by both arrays there are two basic explanations as to how the anomalies are generated. The first, and least plausible, is that topography on the core-mantle boundary conspires to modify the ray path; the second explanation involves lateral and vertical inhomogeneities at the base of the mantle.

The possibility of undulations on the surface of the core was investigated by Vogel (1960) who studied hundreds of PcP determinations and found travel time anomalies that could be interpreted as arising from topographic variations of about ±100 km on the surface of the core. However, such variations are highly susceptible to uncertainties in source depth and location and also to inhomogeneities in the crust and upper mantle. There have been several attempts at explaining that the observed gravitational field of the earth is due in part to such undulations of the core-mantle interface. Hide and Horai (1968) have produced hypothetical contour maps based on a spherical harmonic analysis of the gravity field for degree $n \leq 4$, $n \leq 6$, and $n \leq 8$ being generated by bumps of amplitudes ±4, ±15, and ±66 km respectively,

assuming a density increase of 5.57 to 9.74 g/cm$^3$ across the boundary.

However, it is now known that the radius of the core has been determined to within about 10 km. Jeffreys (1939), Taggart and Engdahl (1968), Johnson (1969), and Buchbinder (1971) obtained core radii of 3473±4 km, 3477 km, 3481±2 km, and 3479±2 km respectively by using PcP phase observations. Jeffreys' value has been used in this study. On the basis of ScS observations Hales and Roberts (1970) have determined the radius to be 3486±5 km. A very sensitive method of measuring not only the radius of the core but also determining the existence of any large scale variations in the shape of the boundary is afforded by multiple reflections such as P3kP, P5kP, P7kP, and so on, where the numeral refers to the number of internal reflections suffered by the compressional wave inside the core. From 20 observations of the P7kP phase Buchbinder (1972) has found a model that agrees to within 1 sec of the data. Therefore, it is apparent that observations of data associated with the core tend to rule out the existence of bumps of more than a few kilometers in amplitude in this boundary. In order to produce the observed phase velocity anomaly ray tracing shows that one would require a depression in the core of nearly 125 km with an increased mantle velocity gradient.

However, this would clearly lead to a negative gravity anomaly which is just the opposite of the observed field and thus eliminates this model.

Davies and Sheppard (1972) have done an extensive study of $dT/d\Delta$ at many distances and azimuths. Their study, using the large aperture seismic array in Montana, indicates a rapid change in $dT/d\Delta$ in the vicinity of the core-mantle boundary near Hawaii, the Galapagos islands, and Iceland. Julian and Sengupta (1973) using travel time evidence have also found anomalous structure beneath Hawaii in this depth range. Some of their rays seem to sample high velocities and some sample low velocities although an explicit spatial distribution with respect to the islands has not been given. Their sampling also indicates that this anomalous structure extends vertically several hundred kilometers.

The results of this work lead to the interpretation that there exists a lateral and vertical heterogeneity near the core-mantle boundary the surface projection of which lies northeast of the island of Hawaii and is approximately 5° in diameter. The high velocity core of this heterogeneity seems to be surrounded by a normal to low velocity aureole which may constitute the plume material as it is heated by the central, possibly rigid, structure causing it to flow upward. The interpretation

assigned to velocities may be justified as a first approximation since the actual azimuthal deviations suffered by the ray from the great circle path are small (<5°). The velocity model used as a standard for this study was Wiggins' (1968) self-consistent velocity and density distribution which was based on model 2 of Birch (1964). A continuous velocity function within the earth's mantle was generated by fitting the discrete values with a cubic spline interpolation formula. The smoothing spline routine (ICSSMU) of the International Mathematical and Statistical Libraries based on the work of Reinsch (1967, 1971) was used in order to avoid numerical instabilities. The geometrical ray integrals (Bullen, 1963) were calculated using a computer program based on the work of Chapman (1971). Upon examination of the three Tonga-Samoa data sets (figures 17a, b, c) it is clear that the experimental phase velocities start to deviate from Birch's model 2 near 84° and continue in this manner smoothly to 91°, beyond which there is a marked increase in the observed velocities and also in their scatter. Birch's model 2 has been perturbed to include a higher velocity gradient between depths of 2371 km and 2861 km (figure 17d) so that a fit to the data in the range 84° to 91° was made. The higher phase velocities for distances beyond 91°

required a sharp increase in mantle velocity to at least 14.7 km/sec between 2861 km and 2898 km. A smooth increase in velocity to 14.7 km/sec at the core-mantle boundary is unacceptable since the shadow would occur at too small an angle and the decay rate of the signal would be increased (Phinney and Alexander, 1969; Chapman and Phinney, 1970). The observations beyond about 89° would not be of a direct P wave but of a trapped interface, or 'head' wave type. Evidence of this is visible in figure 22 which compares an anomalous event with a normal event both from the South Pacific area (Tonga and Solomon islands). The anomalous event exhibits a distinct low frequency precursor which is very much like the head wave precursors generated by Waddington (1973) who has used the Cagniard-de Hoop method to produce synthetic seismograms for this distance range. Of all his velocity-depth models one similar to that shown in figure 17d gives rise to seismograms that are very much alike in appearance to the observed waveforms. The very high phase velocities shown in figures 17b and c for distances less than 88° may be due to reflection (dashed lines) from the high velocity boundary layer.

Both the azimuth-velocity anomaly distribution of figure 20 and the scatter of the phase velocity diagrams of figure 17 indicate that the actual structure

Figure 22. The wave forms of two events, one from the Solomon Islands having a normal phase velocity and one from the Tonga Islands having a high phase velocity. The events are each shown for three stations of VASA.

SOLOMON ISLANDS EVENT: NORMAL

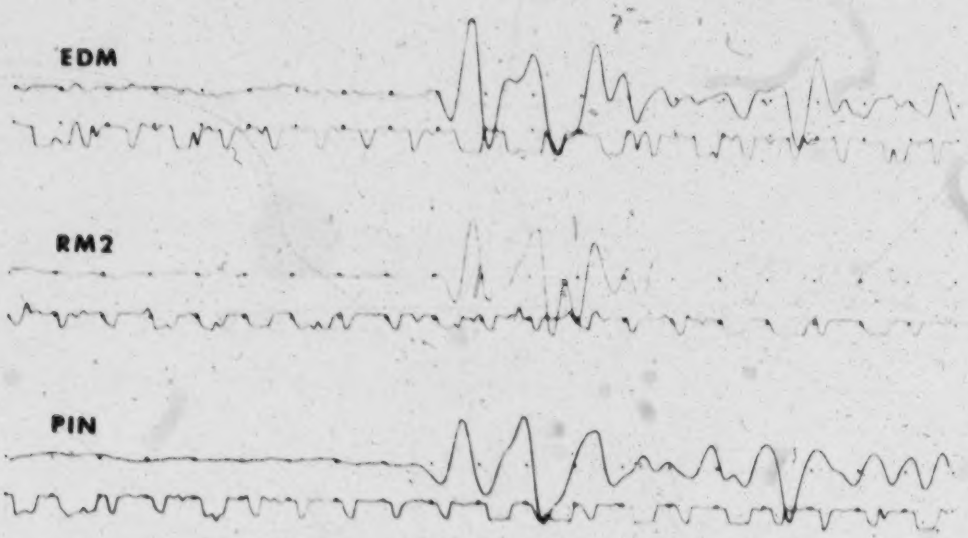


TONGA ISLANDS EVENT: ANOMALOUS

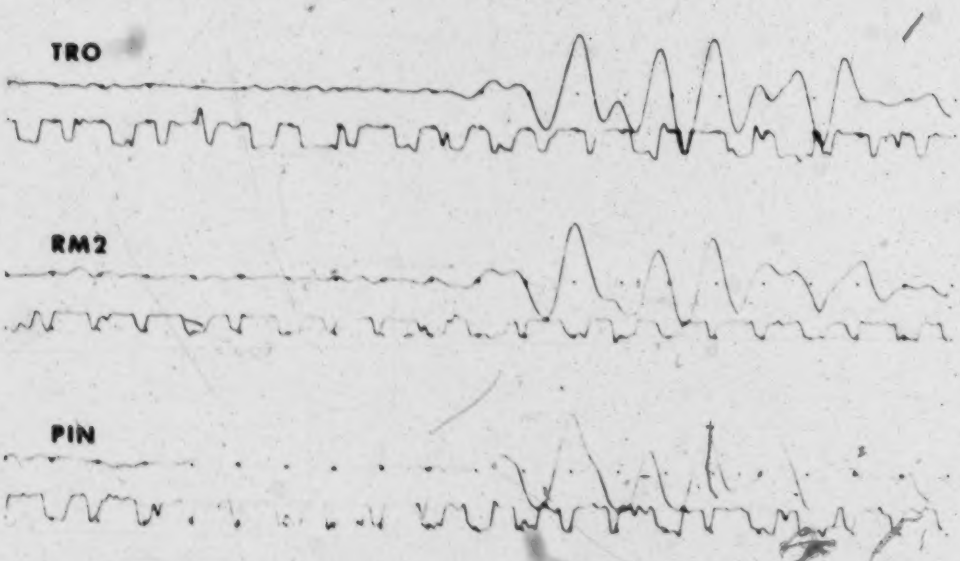


Figure 22.

of the anomalous region is quite complicated and may contain further layering in a vertical sense along with lateral velocity variations as evidenced by the transition from high velocities to low velocities as the structure is traversed. The anomaly is almost certainly no more than 300 km wide and extends upward about 300 to 400 km (from the phase velocity diagrams and the maximum depth of penetration of these rays), although it is very difficult to find an earthquake-receiver system to adequately determine the upper limit on the vertical dimension.

Figure 23 shows a cross section of the earth with the anomaly sketched in at its proposed location at the base of the mantle. The resultant plume is also shown rising through the mantle to the surface where the volcanic islands are generated on the moving Pacific plate. In this diagram are shown a number of seismic rays emanating from what would be a source in the Tonga region.

Figure 23. Sketch of the anomaly at the base of the mantle beneath the Hawaiian linear volcanic chain showing the location with respect to the rays passing through this region.

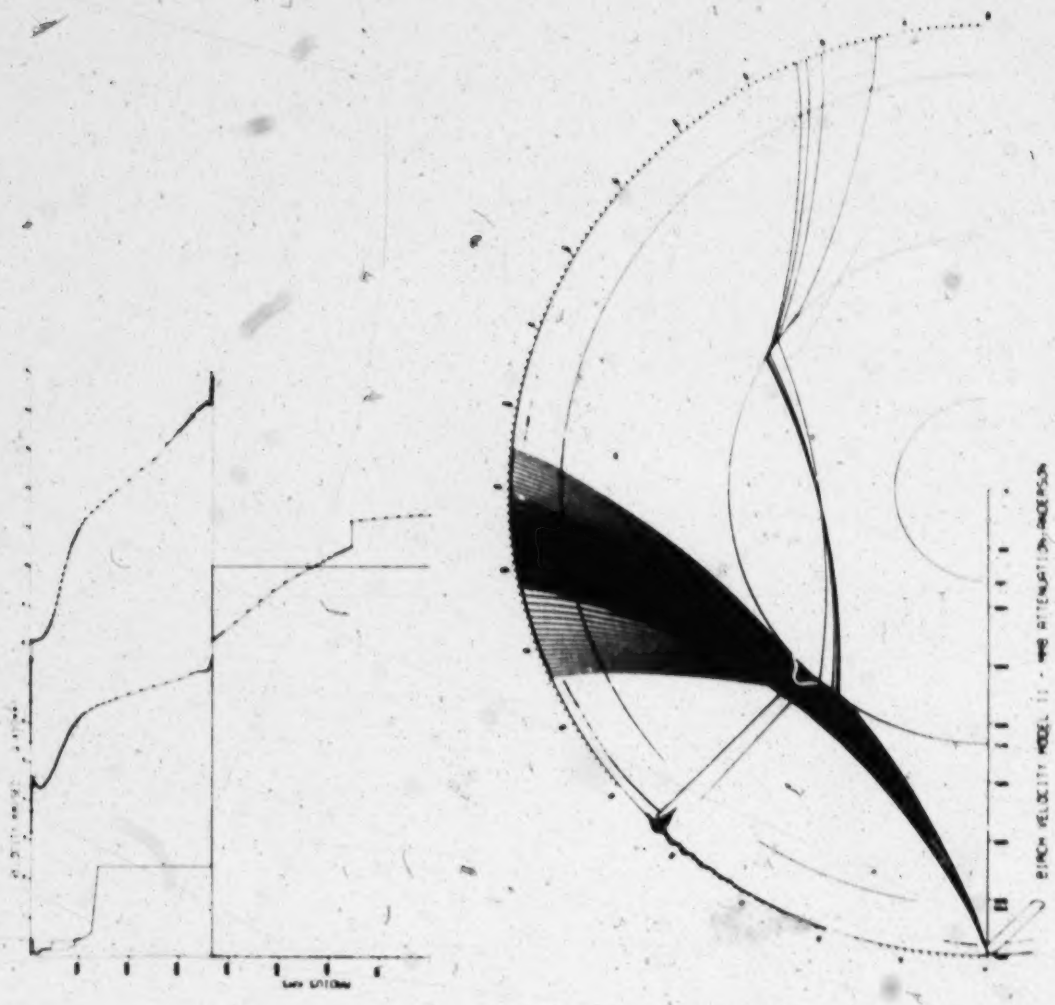

Figure 23.

# CHAPTER IV

## THE HAWAIIAN LINEAR VOLCANIC CHAIN AND ITS POSSIBLE ORIGIN

### 1. Introduction

Upon examining the earth's island systems it becomes apparent that the Hawaiian Islands taken with the Emperor Seamounts are representative of several linear volcanic chains throughout the world. For example one notes the presence of the Austral-Marshall and Tuamoto-Line chains in the Pacific, the Rio Grande and Walvis ridges emanating from Tristan da Cunha and Gough Island in the South Atlantic, and various volcanic provinces in Africa and Europe. In the light of recent mantle hot spot and plume hypotheses it is rather desirable to examine the lower mantle beneath these regions in order to determine the nature and location of any features there. This, combined with crust and upper mantle data, will provide a picture of the nature of the earth over a broad range of depths which is essential for any investigation of the accuracy of the plume hypotheses, their possible worldwide occurrence, and their relationship to the earth's plate tectonic system.

## 2. Surface Description of the Hawaiian Linear Volcanic Chain

Dana (1890) who conducted a rather extensive and detailed survey of the Hawaiian Islands during the middle of the 19th Century recognized the essential volcanic nature of the Hawaiian system and described in some detail the processes of volcanism in this area. He recognized also that the chain is bounded on both sides, at least in the vicinity of Oahu and Molokai, by a more or less continuous trough and that this was probably due to post volcanic subsidence.

Jackson et al. (1972) give a very lucid and extended description of the Hawaiian Archipelago. Theys view the linear chain as being a more or less continuous sequence of shield volcanoes stretching across the Cretaceous sea floor from the island of Hawaii to Midway Atoll and then bending toward the northeast in a line forming the Emperor Seamount chain terminating in the Aleutian trench. Jackson et al. describe the 3500 km ridge as being composed of shield volcanoes rising as much as 9 km above the sea floor and 5 km above sea level having diameters as great as 120 km, all capping the Hawaiian Ridge, a well defined topographic high on the ocean floor bordered on both sides by a moat up to 700 m deep. The individual shields are separated from one another by an average distance of 75 km and began with

the copious eruption of tholeiite (the gentle, free-flowing nature of eruption has led volcanologists to characterize all such eruptions as being of the "Hawaiian type") and was followed by a capping of a much smaller amount of alkalic lava. They point out that projected linear magnetic anomalies cross the Hawaiian chain at angles varying from 30° to 60° and cross the Emperor chain at 80° to 100° showing no change in trend from one side of the chains to the other. The available evidence, they note, indicates that the orientation of the chains has not been influenced by the structure of Cretaceous floor.

3. Geochronology of the Hawaiian-Emperor Chain

The first systematic investigation of the ages of the Hawaiian Islands was done by Dana (1890) who found evidence of a geomorphological nature that the chain became younger from northwest to southeast by observing the progressive state of ruination of the volcanoes in the reverse direction.

This trend has been quantitatively substantiated by McDougall (1964) who has examined samples by K-Ar dating from Kauai to Hawaii and found in general that mean ages for lava deposits decrease toward the southeast (Table 3).

Table 3. Ages of the Hawaiian Islands as a function of distance from the active volcano Kiluea on Hawaii.

| Island | Range of Ages (my) | Distance to Kiluea (km) |
|---|---|---|
| Kauai | 5.6 - 3.8 | 545 |
| West Oahu | 3.4 - 2.7 | 395 |
| East Oahu | 2.5 - 2.2 | 355 |
| West Molokai | 1.8 | 290 |
| East Molokai | 1.5 - 1.3 | 260 |
| West Maui | 1.3 - 1.15 | 220 |
| East Maui | 0.8 | 180 |
| Hawaii - Kohala | 0.68 | 95 |
| - Kiluea | $\geq 0^{+0.4}_{-0.0}$ | 0 |

The trend of increasing age as one moves from Hawaii to Kauai and Midway is supported by Funkhouser et al. (1968) who has also employed K-Ar dating to determine an age of 7.5 my for Nihoa Island and 11.3 my for Necker Island. Paleontological investigations by examination of drill cores on Midway Atoll has established that the island was formed in pre-lower Miocene times having an age greater than 25 my (Ladd et al., 1967). Recent microfossil evidence taken from the most northerly feature of the Emperor Seamount chain, Meiji Seamount, indicates an age of about 70 my (Scholl et al., 1971; Berggren, 1972). Clague and Dalrymple (1973) have examined material dredged from the top of Koko Seamount lying 300 km north of the Hawaiian-Emperor bend, the mean age being determined to be about 46.4 my. They further describe this seamount as having the typical smooth form of the Hawaiian volcanoes probably being formed by the coalescing of several shields.

Thus while extremely sparse as yet, the existing age data from the seamount chain tend to support the trend established by the much more extensively sampled Hawaiian chain.

## 4. Subsurface Data of Hawaii

Gravity data has been examined by Gaposchkin and Lambeck (1971) who have used satellite data to produce

a graph of the global free-air gravity anomalies with respect to the best fitting ellipsoid. The gravity field to the sixteenth degree shows the Hawaiian region within a broad positive anomaly. Kaula (1972) has also noted that the broad positive gravity anomaly around Hawaii is the only one of its type not associated with a spreading center. He further indicates that there are areas having this type of broad positive free-air or isostatic anomaly which seem to be connected with rise formations: Yellowstone, Galapagos, Easter, Eltanin, Balleny, Prince Edward, Bouvet, Iceland, Azores, Afar, Kamchatka, among others.

Pekeris (1935) considers two opposing contributions to gravity anomalies due to the rising part of a convection cell. There is a positive contribution to gravity due mainly to the rise of the upper surface of the crust and there is a negative contribution to gravity on account of the lower density of the matter being pushed up caused by the elevated temperature of the rising stream. He points out, however, that the positive contribution is the larger. McKenzie (1967) states that the long-wavelength harmonics of the gravity field as determined by satellites are not related to shallow crustal or lithosphere effects but are probably related to flow patterns within the deeper mantle, and Runcorn

(1965) argues that departures from hydrostatic equilibrium as evidenced by satellite observations of the geopotential are due to flow within the mantle.

Doell and Cox (1972) have used the idea that the nondipole magnetic field generated within the earth's core may be used to investigate lateral and vertical inhomogeneities at the core-mantle boundary. These variations in the lower mantle will generate differences in the secular changes of the field and the strength of the nondipole field at points of observation on the earth's surface. Doell and Cox point out that it is not attenuation in the lower mantle that gives rise to these variations in the longer period geomagnetic spectrum but rather, lateral changes in the source function. The nature of the source function can be controlled then by properties of the lower mantle by interface coupling with the core through the core-mantle boundary. From paleomagnetic and geomagnetic observatory data they have found a subdued secular variation and a subdued nondipole field in the central Pacific consistent with a pronounced attenuation of the geomagnetic spectrum in the period range 200 to 2000 years. This implies coupling exists between a lateral heterogeneity in the lower mantle and the core resulting in partial extinction of the non-dipole fluctuations in this period range. Limited knowledge of the manner of magnetic field generation in the

core prevents inversion of the data to find a suitable model and also prevents more detailed analysis of other more complex regions.

In a series of papers (Alexander and Phinney, 1966; Phinney and Alexander, 1966, 1969) Phinney and Alexander pursued a study of the core-mantle boundary region by the examination of the spectra of long period diffracted P waves (since these are the first to arrive in the shadow region). The source radiation effects were removed by taking the ratio of the spectra obtained from the vertical ground motion at two stations at least 20° apart and on the same azimuth to the source. The results for waves diffracted at the core-mantle boundary beneath Hawaii showed a broad and pronounced absorption peak in the frequency range 0.03 Hz to 0.04 Hz with smaller peaks being observed at still lower frequencies. Phinney and Alexander considered the kinematics of the deep shadow diffracted wave which travels on the boundary as an interface wave offering sensitivity to lower mantle structure. They attempted to interpret radial and lateral variations observed in terms of layered lower mantle models 30 to 160 km thick having weak absorption peaks in the decay spectrum and noted that for paths where the decay is pronounced this corresponds to a positive velocity gradient of 0.2 km/sec per 100 km. At short periods they suggested that this gradient may be even

greater. For rays diffracted under the Atlantic Ocean off Africa they found no such decay pattern. Although Phinney and Alexander did not produce a particular model to fit their Hawaiian observations they did pioneer the study of lateral and vertical heterogeneities near the core-mantle boundary. Mitchell and Helmberger (1973) using the amplitude ratio of long period SH and $corS$ reflected SH, ScSH/SH (taking the ratio to minimize source and sub-receiver effects), have produced a layered model at the base of the mantle. Comparison of the observed with the synthetic seismograms computed by the Cagniard-de Hoop method indicates that neither the Jeffreys-Bullen nor a negative velocity gradient at the base of the mantle satisfies the observations. Rather, a positive velocity increase of between 0.3 and 0.7 km/sec over a depth range of 40 km to 100 km is deemed necessary. Further restrictions on this model are determined by considering the differential times, ScS-S, for both radial and transverse components, the latter being smaller by an amount explainable by a high velocity region at the base of the mantle 20 to 70 km in thickness having a velocity increase of between 0.3 and 0.5 km/sec. It should be emphasized that the long periods of the shear waves tended to mask lateral heterogeneities (which was desired by the authors). This study, nevertheless, does indicate the existence of positive velocity gradients in this depth range.

## 5. Origins of the Hawaiian Linear Volcanic Chain

Several explanations of the genesis of the Hawaiian linear volcanic chain have been put forward. Wilson (1963) proposed that a source of lava rising from a relatively stagnant center of a plate-driving convection cell in the mantle would puncture the lithosphere depositing volcano producing material in the crust as the plate was pushed along thus forming a line of successively younger volcanoes in a direction opposite to the sense of plate motion.

Dana (1890) using the old supposition that volcanoes arise over the intersection of two faults states that the Hawaiian Islands were formed by two parallel northwest-trending "fundamental rifts" along the course of the island chain with individual volcanoes being generated where these rifts were crossed by northeast-trending fractures. This view was supported by MacDonald and Abbott (1970) whose explanation differs little from Dana's, the orientation of the supposed rift being moderately disrupted by slippage along the intersecting Molokai fault. McDougall (1971) and Green (1971) modify this explanation to a progressive intrusion of magma along lines of structural weakness.

Morgan (1972) gives an explanation similar to that of Wilson (1963) except that his source or "hot spot"

is placed in the lower mantle where it generates a plume of material rising to the earth's surface. Jackson et al. (1972) have reviewed evidence that tremor swarms associated with magmatic movements and eruptions are highly localized being confined to a cylindrical region 25 km in diameter and 25 to 60 km beneath the volcano which is compatible with the shield characteristics of these volcanoes. Hence these extremely localized sources tend to rule out the rather broad upwelling of material inherent in the rift hypotheses. Ryall and Bennett (1968) have examined the crustal structure of Hawaii in great detail finding it complex with the presence of transcrustal fracture zones related to uplift and volcanism. They find, however, 'no evidence for large-scale transcrustal faulting as a controlling factor for volcanism along the Hawaiian Ridge' (Ryall and Bennett, 1968, p.4561). Hill (1969) has done a large amount of seismic refraction work involving the crust and upper mantle underlying the island of Hawaii and has noted that the upper mantle P wave velocity probably decreases beneath Kilauea. Schilling (1973) has indicated that these plume regions such as Iceland and Afar show similar low velocities and that this is to be expected for density-deficient material upwelling from deeper in the mantle.

## 6. Worldwide Nature of Hot Spots and Controversies

Since Wilson (1963) proposed that the genesis of the various volcanic chains is due to the motion of lithospheric plates over hot spots fixed within the mantle with respect to each other, Morgan (1972) has provided a list of 20 probable hot spot locations (figure 24) each being associated with a mantle convection plume. He has noted the worldwide correlation of Hawaii type positive gravity anomalies with the postulated hot spot locations and states that they are symptomatic of rising currents in the mantle: the less dense material of the ascending plume produces a broad negative anomaly which is offset since the surface of the crust is deformed upward causing excess mass to be closer to a satellite passing overhead making the net anomaly positive.

A test of the hypothesized fixed nature of the plumes is whether the directions of the volcanic traces coincide with the direction of instantaneous motion of the plate and whether the age determinations support the accepted plate speeds over the past several million years. Such an investigation has been carried out by Minster, Jordan, Molnar, and Haines (to be published) who have numerically modelled the instantaneous plate tectonics. Their observations of the Pacific, North

Figure 24. Worldwide plume locations (Morgan, 1972).

The abbreviations are as follows:

1. A - Afar
2. Am - Amsterdam
3. Asc - Ascension
4. Az - Azores
5. Bal - Balleny
6. Bou - Bouvet
7. C - Canary Islands
8. C - Comores Islands
9. H - Hawaii
10. Ice - Iceland
11. K - Mount Kenya
12. McD - McDonald
13. PE - Prince Edward
14. Re - Reunion
15. St. H - St. Helena
16. Tr - Tristan de Cunha - Gough

The names in bold face print identify the various tectonic plates.

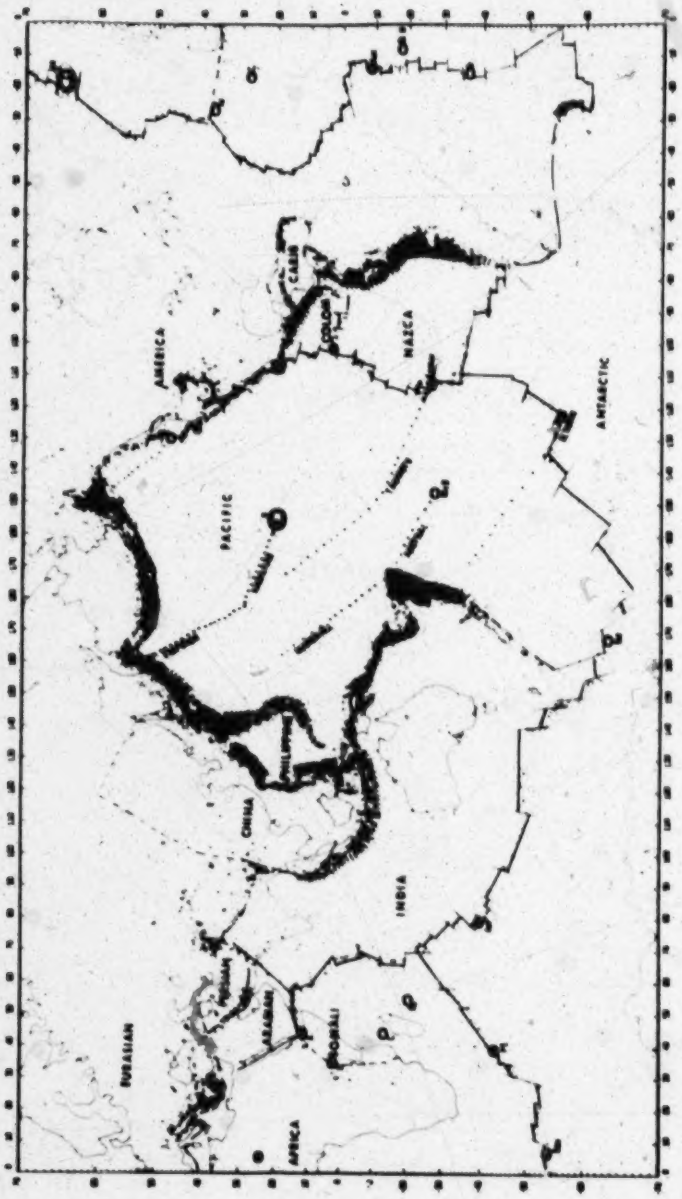
AMERICA
CARIB.
COCOS
NAZCA
ANTARCTIC
PACIFIC
CHINA
INDIA
ARABIAN
SOMALI
AFRICA
EURASIAN
SEISMICITY OF THE EARTH, 1961-1967, ESSA, CDS EPICENTERS,
DEPTHS 000-700 KM.

Figure 24.

American, South American, African, Eurasian, Antarctic, Nazca, and Cocos plates indicate that the fixed plume assumption is indeed in accord with the vast perponderance of data available. In the case of the swiftly moving Pacific plate, for example, their model predicts a present rate of motion over the Hawaiian plume of 8.9 cm/yr at an azimuth of N 66°W compared with their quoted observed azimuth of N 64°W and rates of 10.9 cm/yr (Morgan, 1972), 10 cm/yr (McDougall, 1964), 9 cm/yr (Malahoff and Woollard, 1970) as determined by radiometric dating.

Duncan et al. (1972) have found that assuming the Eurasian plumes are fixed one finds a large discrepancy between the plume polar wander curve and the actual paleo pole positions. They state that this may imply either shifting of the entire lithosphere or a movement of the plumes. McElhinny (1973) has shown that the sum of the vectors (on an equatorial plane) of plate motions relative to the earth's rotation indicates that the lithosphere has not moved as a whole in Tertiary times. The results of Grommé and Vine (1972) who have studied paleo latitude measurements show the same latitude for Midway Atoll as for present day Hawaii within experimental error. Thus, if no true polar wandering has occurred then this plume, and probably the others, must be fixed.

The paradox is resolved, however, since Burke et al. (1973) have shown that Duncan's interpretation of the Eurasian traces upon which his results are based is in error: they describe two plume traces near Iceland-Myvath to Faeroes and Heckla to Rockall Bank, whereas Duncan has incorporated these into a single somewhat meandering trace leading to Scotland; also Burke et al. regard the Central European volcanic province as being composed of two traces both north-south trending in disagreement with Duncan's earlier assumption of one trace running east-west.

Morgan (1972) has given calculations of the vertical and transverse stresses exerted on a plate due to a rising plume. The gravity anomaly created by a plume with a diameter of 150 km is of the order of 20 mgal falling to zero at a distance of 1000 km along the surface which is in accord with actual observations (Kaula, 1973). The shear stress produced on the underside of the plate by such a plume (rising at a rate of 2 m/yr) would be sufficient to drive the plate along at about 5 cm/yr. By suitable choice of viscosity and plume flow rate the total force exerted on the plate can be greater than the resistive drag on the plate bottom and along the edges. The key estimate is the volume of flow of the plume. Conceivably, plumes situated at rise formations may then represent the driving mechanism of the earth's plate tectonic system.

## 7. Conclusion

From the evidence presented in Chapters III and IV it is concluded that the lower mantle does exhibit lateral and vertical inhomogeneities. An anomalous region possessing a high velocity central zone with a normal to low velocity aureole appears to be present just above the core-mantle boundary underneath the island of Hawaii (figure 20, Chapter III). The surface projection of this region, in fact, is located in an area where Jackson et al. (1972) have placed the position of the present Hawaiian plume from geological considerations. The time of formation of this heterogeneity must have been early in the history of the earth's development when the core was being differentiated.

To the present time there has been little satisfactory evidence supporting any of the competing hypotheses for the origin of the Hawaiian linear volcanic chain as outlined in this chapter. Neither a fundamental rift nor a primary source for the lavas has been established. The asthenosphere is an unlikely source in light of plate tectonics and Wilson's (1963) hypothesis and from seismicity studies on the depth of earthquakes and seismic observations of mantle structure there is no indication of a source in the mesosphere. Hence it is indeed possible that a plume, whose surfacing point

lies just northeast of the island of Hawaii, does exist and that its source lies in the anomalous high velocity region at the base of the mantle. This picture, although not unequivocally proven as far as a direct connection between the region at the base of the mantle and the surface is concerned, is not at variance with the $dT/d\Delta$ observations. It should be noted that Shaw and Jackson (1973) prefer an alternate theory for Hawaiian type melting spots. They speculate that shear melting caused by plate motion leads to the formation of a dense residuum which descends to the core-mantle boundary forming a dense high velocity region.

## V. BIBLIOGRAPHY


1. Adams, R.D., 1968. Early reflections of P'P' as an indication of upper mantle structure, Bull. Seism. Soc. Am., 58, 1933.
2. Alexander, S.S., and Phinney, R.A., 1966. A study of the core-mantle boundary using P waves diffracted by the earth's co[illegible]. Geophys. Res. 71, 5943.
3. Anderson, D.L., and Toksöz, M.W., 1963. Surface waves on a spherical earth, 1, J. Geophys. Res., 68, 3483.
4. Anderson, D.L., and Sammis, C., 1970. Partial melting in the upper mantle, Phys. Earth Planet. Interiors, 3, 41.
5. Archambeau, C.B., Flinn, E.A., and Lambert, D.G., 1969. Fine structure of the upper mantle, J. Geophys. Res., 74, 5825.
6. Berggren, W.A., 1972. A Cenozoic time-scale - some implications for regional geology and paleobiogeography, Lethaia, 5, 195.
7. Birch, F., 1964. Density and composition of mantle and core, J. Geophys. Res., 69, 4377.
8. Bolt, B.A., O'Neill, M., and Qamar, A.J., 1969. Seismic waves near 110°: is structure in core or upper mantle responsible?, Geophys. J., 16, 475.
9. Bonilla, M.G., 1970. Surface faulting and related effects. Ch. 3, pp.47-74 in Earthquake Engineering, Ed. R.L. Wiegel, Prentice-Hall, Inc., Englewood Cliffs, N.J., 518 pp.

10. Buchbinder, G.G.R., 1971. Velocity structure of the earth's core, Bull. Seism. Soc. Am., 61, 429.

11. Buchbinder, G.G.R., 1972. Travel times and velocities in the outer core from PmKP, Earth Planet. Sci. Lett., 14, 161.

12. Bullen, K.E., 1963. Theory of Seismology, 3rd ed., p. 119, Cambridge University Press, London.

13. Burke, K., Kidd, F.S.W., and Wilson, J.T., 1973. Plumes and concentric plume traces of the Eurasian plate, Nature, 241, 128.

14. Chapman, C.H., 1971. On the computation of seismic ray travel times and amplitudes, Bull. Seism. Soc. Am., 61, 1267.

15. Chapman, C.H., and Phinney, R.A., 1970. Diffraction of P wave by the core and an inhomogeneous mantle, Geophys. J., 21, 185.

16. Chinnery, M.A., and Toksöz, M.N., 1967. P-wave velocities in the mantle below 700 km, Bull. Seism. Soc. Am., 57, 199.

17. Clague, D.A., and Dalrymple, G.B., 1973. Age of Koko Seamount, Emperor Seamount Chain, Earth and Planetary Sci. Letters, 17, 411.

18. Dana, J.D., 1890. Characteristics of Volcanoes with Contributions of Facts and Principles from the Hawaiian Islands, Sampson Low, Marston, Searle, and Rivington, Ltd., London.

19. Davies, D., and Sheppard, R.M., 1972. Lateral heterogeneity in the earth's mantle, Nature, 239, 318.

20. Davies, D., Kelley, E.J., and Filson, J.R., 1971. Vespa process for analysis of seismic signals, Nature, 232, 8.

21. Duncan, R.A., Petersen, N., and Hargraves, R.B., 1972. Mantle plumes, movement of the European plate, and polar wandering, Nature, 239, 82.

22. Dietz, R.S., 1961. Continent and ocean basin evolution by spreading of the sea floor, Nature, 190, 854.

23. Doell, R.R., and Cox, A., 1972. The Pacific geomagnetic secular variation anomaly and the question of lateral uniformity in the lower mantle, in The Nature of the Solid Earth, edited by E.C. Robertson, pp. 248-284, McGraw-Hill, New York.

24. Doornbos, D.J., and Husebye, E.S., 1972. Array analysis of PkP phases and their precursors, Phys. Earth Planet. Interiors, 5, 387.

25. Engdahl, E.R., and Flinn, E.A., 1969. Waves reflected from discontinuities within the upper mantle, Science, 163, 137.

26. Funkhouser, J.G., Barnes, I.L., and Naughton, J.J., 1968. The determination of a series of ages of Hawaiian volcanoes by the potassium argon method, Pac. Sci., 22, 369.

27. Furumoto, A.S., Campbell, J.F., and Hussong, D.M., 1971. Seismic refraction surveys along the Hawaiian ridge, Kauai to Midway Island, Bull. Seism. Soc. Am., 61, 147.

28. Gaposchkin, E.M., and Lambeck, K., 1971. Earth's gravity field to the sixteenth degree and station coordinates from satellite and terrestrial data, J. Geophys. Res., 76, 4855.

29. Green, D.H., 1971. Composition of basaltic magmas as indicators of condition of origin: application to oceanic volcanism, Roy. Soc. London Phil. Trans. Ser.A, 268, 707.

30. Grommé, S., and Vine, F.J., 1972. Paleomagnetism of Midway Atoll lavas and northward movement of the Pacific plate, Earth Planet. Sci. Lett., 17, 159.

31. Gutenberg, B., 1960. Waves reflected from the 'surface' of the earth: P'P'P'P', Bull. Seism. Soc. Am., 58, 71.

32. Hales, A.L., and Herrin, E., 1972. Travel times of seismic waves, in the Nature of the Solid Earth, edited by E.C. Robertson, pp. 172-215, McGraw-Hill, New York.

33. Hales, A.L., and Roberts, J.L., 1970. Shear velocities in the lower mantle and the radius of the core, Bull. Seism. Soc. Am., 60, 1427.

34. Hide, R., and Horai, K., 1968. On the topography of the core mantle interface, Phys. Earth Planet. Interiors, 1, 305.

35. Hill, D.P., 1969. Crustal structure of the island of Hawaii from seismic-refraction measurement, Bull. Seism. Soc. Am., 59, 101.

36. Hoffman, J.P., Berg, J.W., and Cook, K.L., 1961. Discontinuities in the earth's upper mantle as indicated by reflected seismic energy, Bull. Seism. Soc. Am., 51, 17.

37. Husebye, E.S., 1969. Direct measurement of $dT/d\Delta$, Bull. Seism. Soc. Am., 59, 717.

38. Husebye, E.S., Kanestrøm, R., and Rud, R., 1971. Observations of vertical and lateral P velocity anomalies in the earth's mantle using the Fennoscandian continental array, Geophys. J., 25, 3.

39. Isacks, B., Oliver, J., and Sykes, L.R., 1968. Seismology and the new global tectonics, J. Geophys. Res., 73, 5855.

40. Iyer, H.M., and Healy, J.H., 1972. Teleseismic residuals at the Lasa - USGS extended array and their interpretation in terms of crust and upper mantle structure, J. Geophys. Res., 77, 1503.

41. Jackson, E.D., Silver, E.A., and Dalrymple, G.B., 1972. Hawaiian-Emperor chain and its relation to Cenozoic circumpacific tectonics, Geol. Soc. Am. Bull., 83, 601.

42. Jeffreys, H., 1939. The times of PcP and ScS, Mon. Not. R. Astr. Soc., Geophys. Suppl., 4, 537.

43. Jeffreys, H., and Bullen, K.E., 1958. Seismological Tables, British Association for the Advancement of Science, London.

44. Johnson, L.R., 1967. Array measurements of P velocities in the upper mantle, J. Geophys. Res., 72, 6309.

45. Johnson, L.R., 1969. Array measurements of P velocities in the lower mantle, Bull. Seism. Soc. Am., 59, 973.

46. Julian, B.R., and Sengupta, M.K., 1973. Seismic travel time evidence for lateral inhomogeneity in the deep mantle, Nature, 242, 443.

47. Kanasewich, E.R., Siewert, W.P., Burke, M.D., McCloughan, C.H., and Ramsdell, L., Bull. Seism. Soc. Am., in press.

48. Kaula, W.M., 1972. Global gravity and tectonics, in The Nature of the Solid Earth, edited by E.C. Robertson, pp. 386-405, McGraw-Hill, New York.

49. Ladd, H.S., Tracey, Jr., J.I., and Gross, M.G., 1967. Drilling on Midway Atoll, Hawaii, Science, 156, 1088.

50. MacDonald, G.A., and Abbott, A.T., 1970. Volcanoes in the sea, in The Geology of Hawaii, pp. 281, 441, University of Hawaii Press, Honolulu.

51. McDougall, I., 1964. Potassium argon ages from lavas of the Hawaiian islands, Geol. Soc. Am. Bull., 75, 107.

52. McElhinny, M.W., 1973. Mantle plumes, paleomagnetism, and polar wandering, Nature, 241, 523.

53. McKenzie, D.P., 1967. Some remarks on heat flow and gravity anomalies, J. Geophys. Res., 72, 6261.

54. Malahoff, A., and Wollard, G.P., 1970. Geophysical studies of the Hawaiian ridge and Murray fracture zone, in The Sea, part 2, vol. 4, edited by A.E. Maxwell, pp. 73-131, Interscience, New York.

55. Mitchell, B.J., and Helmberger, D.V., 1973. Shear velocities at the base of the mantle from observations of S and ScS, J. Geophys. Res., 78, 6009.

56. Montalbetti, J.F., 1971. Computer determination of seismic velocities - a review, Canadian Soc. of Exploration Geophysicists.

57. Morgan, W.J., 1972. Deep mantle convection plumes and plate motions, Am. Ass. Petrol. Geol. Bull., 56, 203.

58. Niazi, M., and Anderson, D.L., 1972. Upper mantle structure of western North America from apparent velocities of P waves, J. Geophys. Res., 70, 4633.

59. Oliver, J., and Isacks, B., 1967. Deep earthquake zones, anomalous structures in the upper mantle and the lithosphere, J. Geophys. Res., 72, 4259.

60. Pekeris, C.L., 1935. Thermal convection in the interior of the earth, Mon. Not. Roy. Astr. Soc., Geophys. Suppl., 3, 343.

61. Phinney, R.A., and Alexander, S.S., 1966. P wave diffraction theory and the structure of the core-mantle boundary, J. Geophys. Res., 71, 5959.

62. Phinney, R.A., and Alexander, S.S., 1969. The effect of a velocity gradient at the base of the mantle on diffracted P waves in the shadow, J.Geophys.Res.,74, 4967.

63. Rait, R.W., 1956. Seismic refraction studies of the Pacific Ocean basin, 1, Crustal thickness of the central equatorial Pacific, Geol. Soc. Am. Bull., 67, 1623.

64. Reinsch, C.H., 1967. Smoothing by spline functions, 1, Numer. Math., 10, 177.

65. Reinsch, C.H., 1971. Smoothing by spline functions, 2, Numer. Math., 16, 451.

66. Runcorn, S.K., 1965. Changes in the convection pattern in the earth's mantle and continental drift: Evidence for a cold origin of the earth, Phil. Trans. Roy. Soc., Ser. A, 258, 228.

67. Ryall, A., and Bennett, D.L., 1968. Crustal structure of southern Hawaii related to volcanic processes in the upper mantle, J. Geophys. Res., 71, 4561.

68. Sacks, I.S., 1967. Diffracted P wave studies of the earth's core, 2, Lower mantle velocity, core size, lower mantle structure, J. Geophys. Res., 72, 2589.

69. Schilling, J.G., 1973. Afar mantle plume: rare earth evidence, Nature, 242, 2.

70. Schneider, W.A., and Backus, M.M., 1968. Dynamic correlation analysis, Geophysics, 33, 105.

71. Scholl, D.W., Creager, J.S., Boyce, R.C., Echols, R.J., Fullam, T.J., Grow, J.A., Koizumi, I., Lee, J.H., Ling, H.Y., Supko, P.R., Stewart, R.J., Worsley, T.R., 1971. Deep sea drilling project, Leg 19, Geotimes, 16, 12.

72. Shor, G.G., Jr., 1963. Refraction and reflection techniques and procedure, in The Sea, vol. 3, edited by M.M. Hill, pp. 20-38, Interscience, New York.

73. Sorrells, G.G., Crowley, J.B., and Veith, K.F., 1971. Methods for computing ray paths in complex geological structures, Bull. Seism. Soc. Am., 61, 27.

74. Taggart, J.W., and Engdahl, E.R., 1968. Estimation of PcP travel times and the depth to the core, Bull. Seism. Soc. Am., 58, 1293.

75. Taner, M.T., and Koehler, F., 1969. Velocity spectra - digital computer derivation and applications of velocity functions, Geophysics, 34, 859.

76. Vogel, A., 1960. Über Unregelmässigkeiten der äusseren Begrengung des Erdkerns auf Grund von am Esdkern reflektierten Erdbebenwellen, Gerlands Beitr. Geophys., 69, 150.

77. Whitcomb, J.H., and Anderson, D.L., 1970. Reflection of P'P' seismic waves from discontinuities in the mantle, J. Geophys. Res., 75, 5713.

78. Whitcomb, J.H., 1971. Reflections of P'P' seismic waves from 0 to 150 km depth under the Ninety-East Ridge, Indian Ocean, and the Atlantic-Indian rise, Am. Geophys. Union Monograph, 14, 211.

79. Whitcomb, J.H., 1973. Asymmetric P'P': an alternative to P'd P' reflections in the uppermost mantle, Bull. Seism. Soc. Am., 63, 133.

80. Wiggins, R.A., 1968. Terrestrial variational tables for the periods and attenuation of the free oscillations, Phys. Earth Planet. Interiors, 1, 201.

81. Wilson, J.T., 1963. A possible origin of the Hawaiian islands, Can. J. Phys., 41, 863.

82. Shaw, H.R. and Jackson, E.D., 1973. Linear island chains in the Pacific: the result of thermal plumes or gravitational anchors, J. Geophys. Res., 78, 8634.

# VI. APPENDIX

**********

THIS PROGRAM IS A GENERAL VELOCITY - AZIMUTH SPECTRAL ANALYSIS PROGRAM PRODUCED BY P. R. GUTOWSKI AT THE U. OF ALBERTA.

... LATEST UPDATE -- MAR. 19/73 ...

THE ORIGINAL VELOCITY SPECTRAL ANALYZER WAS GIVEN BY D. DAVIES ET AL.. NATURE 1970. AND FEATURED BEAM FORMING FOR EACH VELOCITY (DELAY AND SUMMATION) AND THEN FOUND THE POWER IN 1 SEC OF BEAM IN 1 SEC INCREMENTS DOWN THE RECORD. THE RESULTING VELOCITY VS. TIME MATRIX WAS THEN CONTOURED AND PLOTTED. THIS METHOD HAS SINCE BEEN SHOWN TO BE RATHER DEPENDENT ON AMPLITUDE VARIATIONS ACROSS THE ARRAY WITH DISTINCT SIDE LOBES APPEARING EVEN FOR LARGE NUMBERS OF SENSORS. THE VELOCITY - AZIMUTH SPECTRAL METHOD (COVESPA) DOES NOT SUFFER FROM THIS DRAWBACK AS IT INVOLVES A COHERENCE FUNCTION GENERATED BY CROSS MULTIPLICATION OF TRACES IN COMBINATIONS OF TWO NOT THE SIMPLE SUMMATION OF THE SENSORS I.E. FOR 5 SENSORS BEAMFORM WOULD LEAD TO THE SUM OF 5 TRACES WHEREAS COVESPA WOULD CROSS MULTIPLY 10 TIMES (5 C 2) AND THUS MAKES MUCH MORE EFFICIENT USE OF THE AVAILABLE DATA REDUNDANCY. IN ADDITION COVESPA SWEEPS NOT ONLY THROUGH VELOCITY AND TIME. BUT ALSO THROUGH AZIMUTH THUS EMPLOYING THE MAXIMUM INFORMATION INHERENT IN ARRAY DATA. FOR A MODERATE NUMBER OF SENSORS THEREFORE. THERE WILL BE VERY LITTLE SIDE LOBE PROBLEM.

**********

INPUT

CARD1 THRU 14 -- ARAY GEOMETRY (DISTANCES AND AZIMUTHS)

CARD15 -- FILE NUMBER OF DATA ON TAPE

CHANNEL 0 - VERTICAL. 1 - NS. 2 - EW

NUMBER OF STATIONS FOR THIS EVENT

LENGTH OF TIME(SEC) INDEX OF CORRELATION MATRIX

STATION NAMES IN LITERAL FORMAT

FORMAT... 4I5 . 5A4

NOTE: NFILE=999 TERMINATES EXECUTION OF PROGRAM

CARD 16 START TIME OF CORRELATION GIVEN IN MIN.

PROGRAM SEARCHES + OR - 10 DEG ON EITHER SIDE

OF THE STARTING AZIMUTH (GEOCENTRIC AZIMUTH)

THE START TIME OF ALL THE RECORDS ARE IN SECONDS

CARD17 LOWER SLOWNESS VALUE IN SEC/DEG

HIGHER SLOWNESS VALUE IN SEC/DEG

SLOWNESS INCREMENT E.G. 0.20 SEC/DEG

NOTE: THESE SHOULD BE CHOSEN SO THAT THERE ARE

LESS THAN 32 SLOWNESSES

CORRELATION LIMIT BELOW WHICH MAXIMA IGNORED

FORMAT 4F10.0

**********

```
C     THIS PROGRAM WILL NOW SEARCH OVER THE SPECIFIED VELOCITY,
C     TIME AND AZIMUTH RANGES GENERATING A SERIES OF COVESPAGRAMS
C     FOR EACH AZIMUTH PRINTING THESE OUT AND PICKING SUCCESSIVE
C     MAXIMA OVER A 5 SEC TIME WINDOW INCREMENTED AT 2 SEC
C     INTERVALS THUS PRODUCING A SERIES OF VELOCITY, TIME, AND
C     AZIMUTH ESTIMATES BY PARABOLA FITTING
C     ********************************************************************

      DIMENSION AZ(7,7),D(7,7),V(5,2000),CC(10,10)
      DIMENSION CCOR(120,31,21),DELTA(10,10),AZM(7),TIMES(5)
      DIMENSION XVEE(31)
      DIMENSION AT(21)
      DIMENSION IA(7),L(10),M(10),ITD(5)
      INTEGER*4 TD(10,10)
      REAL*4 STATNS(5)
      REAL*4 KEYTBL(7)/' DEL',' EDM',' MAR',' PIN',' RM1',
     1' RM2',' TRO'/
      INTEGER*2 IDAT(8192)
      NFLST=1

C     READ ARRAY DISTACES FROM STATION TO STATION

      READ(5,101) D

C     READ ARRAY AZIMUTHS  FORWARD AND BACK
```

```
      READ(5,101) AZ
  101 FORMAT(7F10.6)

      READ NFILE,CHANNEL,NUMBEROF SENSORS,CORRELATION LENGTH,
      AND STATION NAMES

    1 READ(5,100) NFILE,LL,NSTAT,ITSPAN,STATNS
  100 FORMAT(4I5,5A4)
      IF(NFILE .EQ. 999) GO TO 999

      READ START TIME, AZIMUTH, AND TRACE START TIMES

      READ(5,102) TSTRT,AZMTH,TIMES
  102 FORMAT(7F10.0)

      READ LOWER SLOWNESS LIMIT, UPPER LIMIT, CORREL, THRESHOLD

    9 READ(5,105) VL,VU,VDIV,CORLIN
  105 FORMAT(4F10.0)
      IF(NFILE .NE. NFLST) GO TO 401

      IDENTIFY STATIONS

  402 DO 71 I=1,NSTAT
      DO 72 J=1,7
      IF(STATNS(I) .NE. KEYTBL(J)) GO TO 72
      IA(I)=J
      GO TO 71
```

```
 72 CONTINUE
 71 CONTINUE

    GENERATE ALL POSSIBLE COMBINATIONS OF TWO STATIONS

    AN=NSTAT
    NUM=AN*(AN-1.)/2.
    J=1
    K=1
    DO 19 I=1,NUM
    K=K+1
    IF(K .LE. NSTAT) GO TO 11
    J=J+1
    K=J+1
 11 L(I)=J
 19 M(I)=K

    FIND AMOUNT OF DATA TO TAKE FROM TAPE AND WHERE TO START

    TMAX=TIMES(1)
    IMAX=1
    DO 20 I=2,NSTAT
    IF(TMAX .GT. TIMES(I)) GO TO 20
    TMAX=TIMES(I)
    IMAX=I
 20 CONTINUE
    DO 200 I=1,NSTAT
    TDEL=TMAX-TIMES(I)
```

```
      IDELAY=12.5*TDEL
  200 ITD(I)=4*IDELAY
      BLK=TSTRT/2.73067
      MBLK=BLK
      XBLK=MBLK
      TREM=2.73067*(BLK-XBLK)
      IREM=4*IFIX(TREM*750.)
      ITSPAN=ITSPAN+40
      TSPAN=ITSPAN
      ISPAN=12.5*TSPAN
      WRITE(6,814) ITD

  814 FORMAT(5X,'ITD...',5I10)
      WRITE(6,818) BLK,XBLK,TREM,IREM,ISPAN
  818 FORMAT(5X,'...',3F10.4,3I10)
      DO 210 I=1,NSTAT

      READ STATION HEADER FOR THIS EVENT

      READ(8) NF,IEVNT,SYS,STAT
      READ(8,END=220)

      SKIP TO STATION DATA FOR THIS EVENT

  220 CALL SKIP(0,MBLK,8)
      ICOR=0
      READ(8) IDAT
      WRITE(6,820) I
```

```
820 FORMAT(5X,'STATN...I',I10)

    PICK OFF DATA FOR EACH STATION SO THAT ALL TRACES ARE
    ALIGNED IN TIME

    DO 230 J=1,ISPAN
    I4=4*J
    K=I4+IREM+ITD(I)-3+LL+ICOR
    V(I,J)=IDAT(K)
    IF(K .LT. 8189+LL) GO TO 230
    WRITE(6,820) K
    WRITE(6,820) I4
    READ(8) IDAT
    ICOR=-IREM-ITD(I)-I4
230 CONTINUE

    REMOVE DC LEVEL

    DC=0.0
    DO 233 J=1,ISPAN
233 DC=DC+V(I,J)
    DC=DC/FLOAT(ISPAN)
    DO 234 J=1,ISPAN
234 V(I,J)=V(I,J)-DC
    WRITE(6,900) NF,IEVNT,STAT
900 FORMAT(5X,'PARTIAL TAPE HEADER ',2I5,A10)
    WRITE(6,821) DC
821 FORMAT(5X,'DC...',F10.3)
```

```
      CALL SKIP(1,0,8)
210   NFLST=NFLST+2
      ITSPAN=ITSPAN-20
      RAD=3.14159/180.
      IVL=VL*100. + 0.2
      IVU=VU*100. + 0.2
      IVDIV=VDIV*100. + 0.2
      AZML=AZMTH-10.
      AZMU=AZMTH+10.
      IAZML=AZML*10.
      IAZMU=AZMU*10.
      IZ=0
      DO 107 IAZM=IAZML,IAZMU,10
      IZ=IZ+1
      AT(IZ)=FLOAT(IAZM)/10.
      A=AT(IZ)
      AZM(2)=A
      AZM(1)=A+0.17850
      AZM(3)=A-0.648
      AZM(4)=A-0.08083
      AZM(5)=A-1.63950
      AZM(6)=A-1.54783
      AZM(7)=A+0.23184

      CALCULATE DISTANCES FROM STATION TO STATION THE WAVEFRONT
      HAS TO TRAVEL FOR EACH AZIMUTH

      DO 250 I=1,NUM
```

```
      DELTA(L(I),M(I))=D(IA(L(I)),IA(M(I)))*COS(RAD*(AZM(IA(L(I
     1))))-AZ(IA(L(I)),IA(M(I))))
  250 CONTINUE

      FOR THIS AZIMUTH CALCULATE COVESPAGRAM

      IV=0
      DO 306 IVEL=IVL,IVU,IVDIV
      IT=0
      IV=IV+1
      VEX=FLOAT(IVEL)/100.
      IVLIM=IV
      VEE=111.2/VEX
      XVEE(IV)=VEX

      CALCULATE DELAY TIMES FOR EACH 2 STATION COMBINATION
      FOR EACH VELOCITY

      DO 301 I=1,NUM
  301 TD(L(I),M(I))=12.5*(DELTA(L(I),M(I))/VEE)

      STEP DOWN IN TIME ALONG RECORDS DELAYED FOR THIS VELOCITY

      DO 305 ITOR=20,ITSPAN,2
      IOR=12.5*FLOAT(ITOR)
      NEND=12
      IFLAG=0
  304 TCC=0.0
```

```
      IT=IT+1
      IOR1=IOR
      K=1

      CROSS MULTIPLY 1 SEC OF DATA FOR ALL COMBINATIONS AND
      SUM THESE AT THIS TIME

      ************************************************************************

      DO 302 I=1,NUM
      TTCC=0.0
      ANORM1=0.0
      ANORM2=0.0
      DO 303 JJ=1,NEND
      J=JJ-1
      TTCC=TTCC+V(L(I),IOR1+J)*V(M(I),IOR1+J-TD(L(I),M(I)))
      ANORM1=ANORM1+V(L(I),IOR1+J)**2
  303 ANORM2=ANORM2+V(M(I),IOR1+J-TD(L(I),M(I)))**2
      CC(L(I),M(I))=TTCC/(ANORM1*ANORM2)**0.5
      TCC=TCC+CC(L(I),M(I))

      ENTER THIS VALUE INTO MATRIX

      C@OR(IT,IV,IZ)=TCC*2./(AN*(AN-1.))
      IF(L(I+1) .EQ. L(I)) GO TO 302
      IOR1=IOR-TD(L(K),M(K))
      K=K+1
  302 CONTINUE
```

```
      IF(IFLAG .NE. 0) GO TO 305
      IOR=12.5*FLOAT(ITOR+1)
      IFLAG=1
      NEND=13
      GO TO 304
  305 CONTINUE

      ********************************************************************

  306 CONTINUE
      IT=1
      WRITE(6,109) A
  109 FORMAT(5X,'AZIMUTH= ',F10.2,' FOLLOWED BY V-T X-CORR
     1PROFILE'/)
      WRITE(6,110) XVEE
  110 FORMAT(11X,29F4.2/)
      ITSPAN=ITSPAN-20

      WRITE MATRICES

      DO 980 IT=1,ITSPAN
      WRITE(6,981) IT,(CCOR(IT,IV,IZ),IV=1,IVLIM)
  981 FORMAT(1X,I5,5X,40F4.1)
  980 CONTINUE
      ITSPAN=ITSPAN+20
      WRITE(6,983)
  983 FORMAT(////)
  107 CONTINUE
```

```
      ITSPAN=ITSPAN-20

      STEP DOWN MATRICES IN TIME AND PICK MAXIMA ABOVE LIMIT

      ITMAX=0
  692 J=ITMAX+2
      JJ=J+4
      IF(J .GT. ITSPAN-5) GO TO 1
      CMAX=CCOR(1,1,1)
      DO 91 IZ=1,21
      DO 91 IT=J,JJ
      DO 91 IV=1,IVLIM
   91 IF(CCOR(IT,IV,IZ) .GE. CMAX) CMAX=CCOR(IT,IV,IZ)
      IF(CMAX .GE. CORLIM) GO TO 93
      WRITE(6,952) CMAX
  952 FORMAT(5X,'CORREL LESS THAN LIMIT, CMAX= ',F10.3)
      ITMAX=ITMAX+2
      GO TO 691
   93 DO 2 IZ=1,21
      DO 2 IT=J,JJ
      DO 2 IV=1,IVLIM
      IF(CCOR(IT,IV,IZ) .EQ. CMAX) GO TO 3
    2 CONTINUE
    3 CONTINUE
      IF(IV .LE. IVLIM-1 .AND. IV .GE. 2) GO TO 694
      WRITE(6,701) IV,IZ,IT
  701 FORMAT(5X,'MAX. CORREL AT MATRIX EDGE,IV,IZ,IT= ',3I5)
      ITMAX=ITMAX+2
```

```
      GO TO 691
  694 IF(IZ .LE. 20 .AND. IZ .GE. 2) GO TO 693
      WRITE(6,701) IV,IZ,IT
      ITMAX=ITMAX+2
      GO TO 691
  693 ITMAX=IT

      FIT PARABOLAS IN TIME, VELOCITY, AND AZIMUTH


      TWOA=CCOR(IT,IV+1,IZ)+CCOR(IT,IV-1,IZ)-2.*CCOR(IT,IV,IZ)
      B=(CCOR(IT,IV+1,IZ)-CCOR(IT,IV-1,IZ))/2. - TWOA*FLOAT(IV)
      FP=-B/TWOA
      IFP=FP
      APPVEE=XVEE(IFP)+(FP-FLOAT(IFP))*(XVEE(IFP+1)-XVEE(IFP))

      TWOA=CCOR(IT+1,IV,IZ)+CCOR(IT-1,IV,IZ)-2.*CCOR(IT,IV,IZ)
      B=(CCOR(IT+1,IV,IZ)-CCOR(IT-1,IV,IZ))/2. - TWOA*FLOAT(IT)
      TP=-B/TWOA

      TWOA=CCOR(IT,IV,IZ+1)+CCOR(IT,IV,IZ-1)-2.*CCOR(IT,IV,IZ)
      B=(CCOR(IT,IV,IZ+1)-CCOR(IT,IV,IZ-1))/2. - TWOA*FLOAT(IZ)
      FP=-B/TWOA
      IFP=FP
      APPAZM=AT(IFP)+(FP-FLOAT(IFP))*(AT(IFP+1)-AT(IFP))

      T0=TSTRT*60.+20.
      WRITE(6,558) T0
```

```
558 FORMAT(5X,'AT ',F10.5,' SECS DOWN THE RECORD'/)
    WRITE(6,560) CMAX
560 FORMAT(5X,'MAX. CORREL.= ',F10.3)

    WRITE TIME AZIMUTH VELOCITY

    WRITE(6,550) APPVEE,TP,APPAZM
550 FORMAT(5X,'APP. VEL== ',F10.5,' TIME= ',F10.5,' APP. AZM= '
   1,F10.5/)
691 GO TO 692

    ************************************************************


401 CALL SKIP(NFILE-NFLST,0,8)
    IF(NFILE-NFLST .LT. 0) GO TO 501
    NFLST=NFILE
    GO TO 402
501 CALL SKIP(-1,0,8)
    CALL SKIP(1,0,8)
    NFLST=NFILE




999 CALL EXIT
    END
```